

Reversible covalent c-Jun N-terminal kinase inhibitors targeting a specific cysteine by precision-guided Michael-acceptor warheads

Received: 22 August 2023

Accepted: 13 September 2024

Published online: 04 October 2024

Check for updates

Dániel Bálint ^{1,2,11}, Ádám Levente Póti ^{3,4,11}, Anita Alexa ³, Péter Sok ³, Krisztián Albert ³, Lili Torda¹, Dóra Földesi-Nagy³, Dániel Csókás⁵, Gábor Turczel ⁶, Tímea Imre⁷, Eszter Szarka³, Ferenc Fekete⁸, Isabel Bento⁹, Márton Bojtár ¹⁰, Roberta Palkó¹, Pál Szabó ⁷, Katalin Monostory⁸, Imre Pápai⁵, Tibor Soós ¹ & Attila Reményi ³

There has been a surge of interest in covalent inhibitors for protein kinases in recent years. Despite success in oncology, the off-target reactivity of these molecules is still hampering the use of covalent warhead-based strategies. Herein, we disclose the development of precision-guided warheads to mitigate the off-target challenge. These reversible warheads have a complex and cyclic structure with optional chirality center and tailored steric and electronic properties. To validate our proof-of-concept, we modified acrylamide-based covalent inhibitors of c-Jun N-terminal kinases (JNKs). We show that the cyclic warheads have high resilience against off-target thiols. Additionally, the binding affinity, residence time, and even JNK isoform specificity can be fine-tuned by adjusting the substitution pattern or using divergent and orthogonal synthetic elaboration of the warhead. Taken together, the cyclic warheads presented in this study will be a useful tool for medicinal chemists for the deliberate design of safer and functionally fine-tuned covalent inhibitors.

While covalent targeting has long played a subordinate role in drug developments, there has been a recent surge of interest in the application of the so-called targeted covalent inhibitors (TCIs) in potent and selective inhibition of kinases¹. Of the 62 protein kinase inhibitors that are approved by the Food and Drug Administration, over half a dozen of them are TCI, thus, this paradigm shift has become the basis of many current drug discovery programs². TCIs are typically evolved from optimized reversible ligands, which are then endowed with an

electrophilic reactive group to form a covalent bond with the targeted enzyme via a specific, noncatalytic residue (mainly cysteine on kinases)^{3–5}. This unique combination of correct positioning and covalent binding leads to a drug with exceptional potency and selectivity. Moreover, this approach has also been effective in counteracting resistance developed against some broadly used classical cancer drugs^{6–9}.

The cysteine-targeting acrylamides have become the gold standard for warheads in TCIs, especially in the kinase field, thanks to their

¹Organocatalysis Research Group, Institute of Organic Chemistry, Research Centre for Natural Sciences, 1117 Budapest, Hungary. ²Hevesy György PhD School of Chemistry, Eötvös Loránd University, 1117 Budapest, Hungary. ³Biomolecular Interaction Research Group, Institute of Organic Chemistry, Research Centre for Natural Sciences, 1117 Budapest, Hungary. ⁴Doctoral School of Biology, Eötvös Loránd University, 1117 Budapest, Hungary. ⁵Theoretical Chemistry Research Group, Institute of Organic Chemistry, Research Centre for Natural Sciences, 1117 Budapest, Hungary. ⁶NMR Research Laboratory, Centre for Structural Science, Research Centre for Natural Sciences, 1117 Budapest, Hungary. ⁷MS Metabolomic Research Laboratory, Centre for Structural Science, Research Centre for Natural Sciences, 1117 Budapest, Hungary. ⁸Metabolic Drug-interactions Research Group, Institute of Molecular Life Sciences, Research Centre for Natural Sciences, 1117 Budapest, Hungary. ⁹European Molecular Biology Laboratory, EMBL, Hamburg, Germany. ¹⁰Chemical Biology Research Group, Institute of Organic Chemistry, Research Centre for Natural Sciences, 1117 Budapest, Hungary. ¹¹These authors contributed equally: Dániel Bálint, Ádám Levente Póti. e-mail: soos.tibor@ttk.hu; remenyi.attila@ttk.hu

attenuated reactivity toward nucleophiles of the biological matrix and the relative ease of their synthetic elaboration¹⁰. Nevertheless, it has become apparent during their usage that these open-chain electrophilic ligands could inhibit not only kinases, but also other proteins and elicit time-dependent off-target reactivity^{11,12}. These may lead to increased idiosyncratic drug reactions, enhanced risk of haptenization and therefore these acrylamide-tagged TCIs might increase the risk of side-effects. Furthermore, an additional problem could potentially arise as cells contain free thiol nucleophiles (e.g., glutathione/GSH) in a concentration that is often many orders of magnitude higher than any targeted sulfhydryl functionalities^{3,5}. This competitive reactivity may evoke depletion of covalent inhibitors by GSH.

These challenges have triggered the development of various approaches to solve or mitigate the inherent shortcomings of previously developed acrylamide-based covalent warheads⁴. One of the most promising advances in this field was the introduction of reversible inhibitors which possess more reactive but reversible cyanoacrylamide warheads^{13,14}. In this modification, however, the enhanced reactivity toward GSH may still result in reduced effective concentration of TCIs. Additionally, the covalent fragment screening discovery approach, which puts the emphasis on the electrophile-first concept instead of optimizing the noncovalent moiety for a given target, has started to emerge and it is now facilitated by the development of chemoproteomic platforms¹⁵.

Mitogen-activated protein kinases (MAPK) are ubiquitous regulators of cellular physiology. Increased extracellular signal-regulated kinase (ERK1/2) activity is a hallmark of cancer due to its pivotal role in promoting cell growth^{16–18}. Although up-regulation of p38 or c-Jun N-terminal kinase (JNK) activity is also known to be associated with specific cancers, these kinases are better known to be associated with acute or chronic inflammation due to their pivotal role in regulating cell death^{19–22}. There are three distinct genes (*Jnk1*, *Jnk2*, and *Jnk3*) with about ten different isoforms generated through alternative splicing: the predominant JNK1 and JNK2 isoforms are expressed ubiquitously while JNK3 is expressed primarily in the nervous system²³. JNKs are activated by phosphorylation at their activation loop by MAPK kinases (MAP2K) such as MKK4 and/or MKK7 and regulate their downstream substrates by phosphorylation. For example, the c-Jun and ATF2 transcription factors are phosphorylated by JNK at Ser63/73 and Thr69/71, respectively. JNKs are activated when cells are exposed to stress conditions or cytokines, while they are activated less to exposure to growth factors. Hyperactivation of JNK signaling is common in several disease states including cancer, inflammatory, and neurodegenerative diseases. Based on genetic and pharmacological studies in animal models, JNK inhibitors have anti-inflammatory and neuroprotective effects²³. Specific blocking of JNK activity could be particularly important in treating diseases such as Alzheimer's and Parkinson's diseases, asthma, diabetes, and rheumatoid arthritis. Moreover, selective JNK inhibition would likely have a positive role on neuron regeneration/repair after injury²⁴. Thus, JNK is an attractive target for therapeutic intervention with small molecule kinase inhibitors. As a result, various inhibitors have been developed; however, limitations are noted with these inhibitors including lack of specificity or cell toxicity²⁵. JNKs play critical roles in development and homeostasis, and complete and sustained JNK inhibition may not be desirable²⁶. To date, there are no direct JNK inhibitors approved for use in human therapies.

To block JNK activity selectively, an ATP binding scaffold – developed from imatinib – had formerly been linked to an acrylamide warhead²⁷. These compounds selectively target a specific cysteine through covalent bond formation; this residue is conserved in JNK1-3 and is unique among MAPKs (cysteine 154 in JNK3, cysteine 116 in JNK1 or JNK2). The inhibitors – where the most selective JNK inhibitor was called JNK-IN-8 and will be referred to as such henceforth – were shown to bind to JNK irreversibly. Thus, JNK-IN-8 proved to be a promising JNK-specific kinase inhibitor. Nevertheless, the foreseeable formation

of irreversible C-S cysteine adducts – formed by an acrylamide warhead – raises concerns about potential unwanted off-target effects and about the half-life in a biological environment (e.g., in the presence of various S, N nucleophiles; 1–10 mM GSH)²⁸.

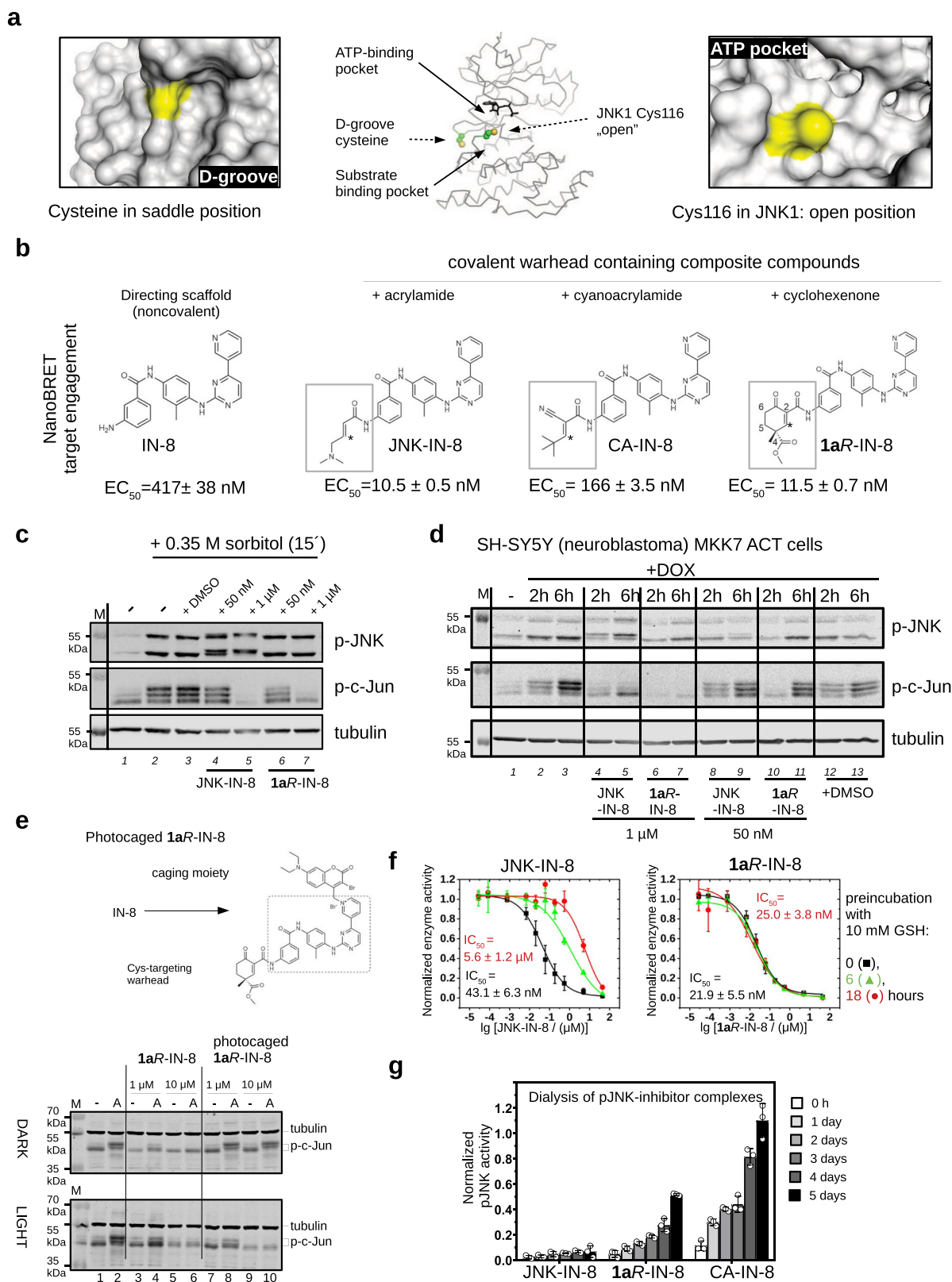
In this work we show through covalent warhead modification of JNK-IN-8 that our recently identified class of cyclic, tunable, and reversible covalent warheads can overcome many shortcomings of previously utilized open-chain warheads²⁹. First we compare JNK inhibitors with a cyclohexenone/pentenone warhead scaffold with other formerly known open-chain Michael acceptor containing compounds and demonstrate that composite inhibitors with a cyclic warhead may have beneficial properties. We show that the inhibitors form a reversible covalent adduct with the target cysteine on JNKs and that inhibitor residence time can be fine-tuned by adjusting the electronic properties and/or steric crowding around the Michael acceptor. In addition to the specificity of the so-called directing group responsible mainly for classical noncovalent binding in the ATP-pocket, the cyclic warhead endows composite drugs with increased kinase and JNK isoform specificity. Finally, we showcase the translational potential of the reversible covalent warheads and underscore their significance in the development of specific reversible covalent inhibitors.

Results

JNK inhibitors with different chemical warheads

A reversible warhead could provide a better alternative to an irreversible electrophile (e.g., acrylamide), particularly if one considers that unwanted cross-reactions in cells, tissues, or in the body are likely to be more devastating if happened through irreversible covalent bond formation. Despite the advances in reversible warhead development, however, there is still a need to broaden the list of easily available and effective warheads. Thus, we envisioned that development and incorporation of warheads with tunable reactivity and enhanced 3D shape might result in more effective and selective inhibitors. In an electrophile-first discovery approach targeting the common MAPK D-groove cysteine via a C-S covalent bond, we identified a class of cyclic, Michael acceptor-based, reversible covalent warhead with a terpenoid-like structure²⁹. Owing to their special structural feature, a state of frustration was expected to emerge, as enhanced steric crowding (substituents of C4 (γ)) around the reactive β -position can hamper Michael-adduct formation with thiol-groups. Additionally, the presence of nearby electron-withdrawing groups is expected to counteract the effect of steric shielding, thus the binding properties (affinity, kinetics and specificity) could be custom-engineered. Gratifyingly, this frustrated state in these warheads allowed the development of cysteine targeting drugs with (a) higher selectivity compared to open-chain (acyclic) covalent inhibitors with an acrylamide warhead and (b) prominent GSH tolerance. Further practical advantage of these warheads is that they can be easily elaborated further using various orthogonal synthetic methods. Thus, the previously used late-stage, appendage approach to introduce acrylamide warheads can be circumvented. Potentially, due to their more complex three-dimensional shape, the cyclic structure of our warheads allows the development of more selective and improved cysteine targeting drugs.

In contrast to free solvent exposed thiols, for example in glutathione, the sulfhydryl group of a cysteine from a protein domain is usually located in a more specific chemical environment: surface topography and the chemical nature of the neighboring amino acid side chains will affect the intrinsic capacity of the α,β -unsaturated Michael acceptor (C3) to form the covalent bond. The thiol of Cys116 in JNK1 is more accessible compared to the MAPK D-groove cysteine (Fig. 1a). Therefore, we envisioned that the advantageous feature of our cyclic warhead designs may also be exploited in the inhibition of JNKs. Indeed, NanoBRET target engagement assay in live HEK293T cells showed that the irreversible (acrylamide) JNK-IN-8 and the reversible (cyclohexenone) **1aR**-IN-8 performed similarly (~ 10 nM),



while reversible cyanoacrylamide-based CA-IN-8 was a weaker JNK binder (~ 200 nM); and, as expected, the ATP binding moiety without any warhead was less effective (~ 500 nM) (Fig. 1b and Supplementary Fig. 1).

Next, we assessed the inhibitory capacity of JNK-IN-8 and 1aR-IN-8 in cells on the JNK pathway. First, HEK293T cells were treated with sorbitol which is known to activate the JNK dependent signaling

pathway³⁰. Both inhibitors efficiently blocked JNK mediated c-Jun phosphorylation when added in 1 μ M concentration while JNK activation was unaffected. Since JNK-IN-8 binding to JNK is irreversible, the electrophoretic mobility of JNK on SDS-PAGE was changed after inhibitor binding. In contrast, 1aR-IN-8 treatment did not affect the electrophoretic mobility of JNK, suggesting that the binding of this inhibitor to JNK is indeed reversible (Fig. 1c). In further experiments we

Fig. 1 | JNK inhibitors containing different chemical warheads. **a** Position of Cys116 in JNK1 compared to the MAPK D-groove cysteine. Left panels show the ERK2 D-groove in surface representation with Cys161 highlighted in yellow (PDB ID: 2ERK). This cysteine, similarly to other MAPK D-groove cysteines from p38 α and JNK1, is more buried since it is located in a less accessible (saddle) position compared to the JNK unique cysteine (Cys116 in JNK1) located next to the ATP-pocket, which is more open. The middle panel shows the relative position of these two cysteines on JNK1 (cysteine side-chain atoms are shown with spheres), while the panel on the right shows the JNK1 surface area around Cys116 (colored in yellow). **b** Comparison of three covalent JNK inhibitors comprised of the IN-8 ATP-pocket binding moiety and a Michael acceptor based warhead (acrylamide – irreversible, cyanoacrylamide – reversible, and cyclohexenone – reversible; * indicates the Michael acceptor carbon (β or C3) forming the C-S bond; the numbering of carbon atoms in the cyclohexenone ring is indicated: C2 and C4 contain electron-withdrawing amide or ester groups increasing the reactivity of C3; C4 is an asymmetric center and the IN-8 directing group is linked to C2 via an amide). The EC₅₀ values of JNK1 binding were measured in live HEK293 cells using the NanoBRET target engagement assay (the values show the mean and parameter error estimates are from weighted least squares method; $n = 2$, independent experiments, see Supplementary Fig. 1). **c** The impact of JNK-IN-8 and **1aR**-IN-8 on sorbitol stimulated JNK and c-Jun phosphorylation in HEK293T cells. Cells were stimulated with sorbitol for 15 min which gives robust JNK activation. ‘-’ indicates no treatment with inhibitors and +DMSO indicates treatment with DMSO used in the same amount (0.1%) as an organic solvent for the inhibitors. Inhibitors were added 2 h before stimulation and blots are representative of two independent experiments. Note the changed electrophoretic mobility of JNK in the presence of JNK-IN-8, indicating irreversible JNK–JNK-IN-8 binding (compare lane 4–5 with the other lanes). (p-JNK: western blot, WB, signal with phosphoJNK antibody; p-c-Jun: WB with phospho-c-Jun (Ser73) antibody where MAPK mediated c-Jun phosphorylation results in differently phosphorylated phospho-c-Jun (p-c-Jun) species with different electrophoretic mobility; the fastest migrating band is the least phosphorylated; Tubulin: WB with anti-tubulin antibody which serves as the load control; M: molecular

marker). **d** Effects of JNK-IN-8 and **1aR**-IN-8 on c-Jun phosphorylation in an engineered neuroblastoma cell line (SH-SY5Y MKK7 ACT). Phosphorylation of JNK (p-JNK) was stimulated by 2 or 6 h of doxycycline (DOX) treatment and blots are representative of two independent experiments. **e** Photocaged JNK inhibitor for light-controlled regulation of JNK activity. **1aR**-IN-8 was linked to a photolysable moiety via its pyridine nitrogen, which blocked its capacity to bind into the JNK ATP-pocket. HEK293T cells were unstimulated (-) or stimulated with 10 μ M anisomycin (A) to turn JNK on. One set of experiment was carried out in the dark (DARK), while in the parallel experiment cells were illuminated briefly with 450 nm blue LED light (LIGHT) but otherwise also kept in the dark. The original inhibitor and its photocaged version were added in 1 or 10 μ M concentrations and JNK-mediated c-Jun phosphorylation was monitored by western blots (and the panel shows a representative set of two independent experiments). Notice that the photocaged inhibitor blocks c-Jun phosphorylation only in LIGHT but not in DARK (compare Lane 7–10 between the upper and the lower panels). (tubulin was used as the load control; lower and upper bands show the position of hypophosphorylated or hyperphosphorylated c-Jun, respectively; p-c-Jun.). **f** Stability in a nucleophile rich environment. The inhibitory potential of JNK-IN-8 and **1aR**-IN-8 were tested using the in vitro PhALC assay after pre-incubating the compounds for different amounts of time in 10 mM GSH (see Methods). In contrast to JNK-IN-8, the effect of **1aR**-IN-8 on JNK is apparently intact since it forms only a weak and transient reversible covalent adduct with GSH. Data show the mean value and error bars show SD ($n = 3$, independent experiments). **g** Results of in vitro dialysis experiments. 50 nM phosphorylated JNK1 (pJNK1) was incubated with 10 μ M inhibitor for 1.5 h, then samples were loaded into dialysis tubes and dialyzed in 50 mM HEPES pH = 7.4, 100 mM NaCl, 5 mM MgCl₂, 2 mM DTT. The samples before the start of the dialysis experiment (0 h) and after the indicated times (1, 2, 3, 4, 5 days) were tested for enzymatic activity using the PhALC assay ($n = 3$; independent experiments; data show the mean and error bars show SD). The control sample (used for normalization) was treated the same way but no inhibitor was added in the incubation step before the dialysis experiment. Source data are provided as a Source Data file.

used an engineered human neuroblastoma cell line (SH-SY5Y MKK7 ACT) where specific JNK pathway activation was triggered by the addition of an artificial inducer (doxycycline). This cellular system allows specific activation of JNKs while leaving other MAPK pathways unaffected³¹. JNK-mediated c-Jun(Ser73) phosphorylation was examined after 2 or 6 h of doxycycline (DOX) treatment, where longer DOX induction triggered higher JNK activity flux. Experiments with inhibitors added in 50 nM or 1 μ M concentrations showed that both compounds can block c-Jun phosphorylation (Fig. 1d).

Next, we devised a chemical biological strategy to demonstrate that the effects of the warhead (**1aR**) on c-Jun phosphorylation in the context of the composite inhibitor (**1aR**-IN-8) indeed depends on JNK ATP-pocket binding, as this would be naturally anticipated. The crystal structure of the acrylamide warhead containing inhibitor bound to JNK3 (PDB ID: 3V6S) showed that the pyridine ring of IN-8 is deeply buried in the ATP-pocket. To achieve light-controllable JNK activity, a photoactivatable version of the **1aR**-IN-8 compound was synthesized. The recently introduced 3-bromo-7-diethylaminocoumarin photo-removable protecting group was selected for caging the pyridine nitrogen of IN-8 via quaternization to reduce binding into the narrow ATP-pocket due to steric blocking³². This photocage permits efficient photorelease of the pyridines upon blue light (450 nm) irradiation generating in this case the original inhibitor in situ for JNK binding (Supplementary Fig. 2). HEK293 cells were treated with anisomycin that turned JNK and thus c-Jun phosphorylation on, and the latter was found to be similar under dark or upon illumination as expected. This demonstrates that the light-activation protocol is neutral to cells. Addition of 1 or 10 μ M free inhibitor (**1aR**-IN-8) greatly reduced or eliminated the effect of anisomycin under both dark and light-activation conditions. More importantly, cells treated with the photocaged inhibitor displayed c-Jun phosphorylation blockade only upon blue light illumination (Fig. 1e). This experiment shows that the inhibitory capacity of **1aR**-IN-8 directly depends on JNK ATP-pocket

engagement in cells, as expected from a JNK-specific ATP-competitive inhibitor.

We also examined the inhibitory capacity of irreversible JNK-IN-8 and reversible **1aR**-IN-8 after exposing them to high amounts of GSH. When these two compounds were incubated in the presence of 10 mM GSH for 6 or 18 h under physiological conditions before adding them into the in vitro kinase assay (PhALC), the IC₅₀ of JNK-IN-8 drastically dropped but **1aR**-IN-8 stayed similarly active in blocking MAPK activity (Fig. 1f). These experiments demonstrate that **1aR**-IN-8 stays functionally intact even after 18 h of incubation in 10 mM GSH, while JNK-IN-8 becomes inactive and its efficacy dramatically drops within a few hours. This latter is due to irreversible covalent adduct formation with GSH based on an analysis with electrospray mass spectrometry (Supplementary Fig. 3). Note that the GSH–**1aR**-IN-8 adduct also forms, which we could only detect by shortening the LC step prior to electrospray mass spectrometry (see Supplementary Fig. 3). Moreover, the covalent adduct of **1aR**-IN-8 with beta-mercaptoethanol (BME) was also detected by ¹H NMR, and a titration experiment indicated the K_{chem} to be ~1 mM for the free thiol (Supplementary Fig. 4). This value was corroborated by an additional electronic circular dichroism measurement using a truncated anilide derivative (the K_{chem} value of **19'S** + BME reaction by EDC titration was also found to be ~1 mM)²⁹. In brief, GSH does not lower the effective concentration of the developed reversible covalent inhibitor since their adduct is transient and its affinity is low (~mM) compared to the thiol adduct forming on the target (JNK) with higher affinity (~low nM) and with a greatly decreased k_{off}.

Next, the off-rate of phosphorylated JNK1–JNK-IN-8, –**1aR**-IN-8, and –CA-IN-8 complexes were examined in an in vitro dialysis experiment. JNK-inhibitor complexes were preformed and then dialyzed up to 5 days. The reversible nature of the JNK1–**1aR**-IN-8 complex, in contrast to the irreversible JNK1–JNK-IN-8 complex, was also confirmed by these experiments since some enzymatic activity of JNK1

(~50%) could be regained if the enzyme had bound to **1aR**-IN-8 but not when to JNK-IN-8. Moreover, faster recovery of JNK activity upon dialysis indicated that the off-rate of the reversible cyanoacrylamide based CA-IN-8 inhibitor is faster (Fig. 1g).

Overall, these *in vitro* experimental results suggest that **1aR**-IN-8 might be a superior JNK inhibitor, due to its reversible cysteine targeting, resilience to GSH, and its similar *in-cell* potency compared to JNK-IN-8, or to its more promising properties compared to the cyanoacrylamide based reversible covalent reference compound (CA-IN-8).

Cyclic Michael acceptor based reversible covalent warheads

Cyclohexenone/pentenone scaffolds provide a platform for controlling intrinsic reactivity: the electronic or steric properties and ring strain could all be modified. We synthesized a set of JNK inhibitors that all contained the same ATP-pocket binding moiety (IN-8) but had different warheads. The warheads were the following: acrylamide – acyclic irreversible (JNK-IN-8)²⁷, cyanoacrylamide (CA) – acyclic reversible, and cyclohexenone/pentenone – cyclic reversible (**1aR**, **1aS**, **2**, **3**, and **4**). These were linked to IN-8 in the same way so that the electrophilic carbon (C3) atom of the α,β -unsaturated carbonyl system could selectively target a surface cysteine located next to the ATP-pocket (Cys116 in JNK1). We also generated two additional **1aR**-IN-8 derivatives, in which the ATP-pocket binding moiety was linked to the cyclic warhead scaffold via an additional methylene group (**1a'R**-IN-8), making the distance between these two presumably less optimal, and this was further modified by changing the amide to an ester group at C2 (**1a''R**-IN-8; thus the latter has a more reactive Michael acceptor). Finally, two more enantiomeric pairs – similar to **1aR**/**1aS**, but distinct in one of the substituent groups at C4 – were synthesized: **5S**/**5R** or **6S**/**6R**, containing a sterically more demanding isopropyl or a C4-C6 bridged skeleton instead of the methyl group, respectively (Table 1). These compounds thus display different tactics to fine-tune the covalent reactivity of the warhead: either increasing sterical crowding (**5**) or constraining the flexibility of the cyclohexenone ring (**6**), which could both indirectly affect the axial-equatorial stereochemical transition at C3 upon C-S covalent bond formation³³. Note that the results of the different assays shown in Table 1 may not be directly compared since they report on the performance of the inhibitors under different scenarios. The *in vitro* PhALC assay or the cell-based NanoBRET target engagement assay monitors only JNK1 specific effects under clean or more competitive conditions, respectively, while the two p-c-Jun assay reports on overall JNK inhibition in the used cell line.

The crystal structure of JNK1-**1aR**-IN-8, **1aS**-IN-8, and **1a'R**-IN-8 complexes were next determined to confirm the formation of the covalent adduct (Table 2). Comparison of these structures suggests that the cyclohexenone core may be used as a platform to orient extra moieties, attached at C4 for example, towards different regions in the wide substrate binding crevice (Fig. 2a). To demonstrate that specific covalent bond formation contributes to binding, JNK-inhibitor complex formation was examined by SPR using wild-type JNK1 or the C116S mutant. This showed that the warheads indeed work as covalent anchors if C116 is intact and thus they decrease the k_{off} as expected (Fig. 2b).

Intrinsic reactivity and binding kinetics

To analyze the contribution of the warheads of IN-8-based JNK inhibitors more rigorously, the binding kinetics of different composite inhibitors were further examined by SPR and the results were quantitatively analyzed (Supplementary Fig. 5). For the latter, a 2-step reversible kinetic model was established (Fig. 3). The reversible binding scheme included the formation of the noncovalent kinase-inhibitor (K:I) complex as well as the covalent adduct (K:I^{COV}). The association and dissociation of K:I are described by the k_1 and k_2 rates, while the formation of K:I^{COV} from K:I or the formation of K:I from K:I^{COV} are

Table 1 | Summary of *in vitro* JNK1 PhALC (with 10 mM GSH), cell-based JNK1 NanoBRET target engagement (HEK293) and p-c-Jun EC₅₀ measurements (SH-SY5Y MKK7 ACT cells)

	R ₁	PhALC IC ₅₀ /(nM)	NanoBRET EC ₅₀ /(nM)	HTRF p-c-Jun(S63) EC ₅₀ /(nM)	Western blot p-c-Jun (S73) EC ₅₀ /(nM)
IN-8		3805 ± 402	417 ± 38	2127 ± 135	8975 ± 2680
IN-8a		5333 ± 232	x	6792 ± 256	n.a.
JNK-IN-8		44 ± 6	10.5 ± 0.5	88 ± 8	760 ± 120
CA-IN-8		318 ± 45	166 ± 35	4970 ± 620	8624 ± 1973
1aR -IN-8		22 ± 6	11.5 ± 0.7	135 ± 15	660 ± 100
1aS -IN-8		30 ± 5	3.3 ± 1.7	65 ± 7	320 ± 120 ^a
1a'R -IN-8		225 ± 17	1060 ± 150	747 ± 247	4320 ± 1380
1a''R -IN-8		349 ± 24	650 ± 180	644 ± 110	7330 ± 3600 ^a
2 -IN-8		780 ± 159	76 ± 30	616 ± 169	3350 ± 370 ^a
3 -IN-8		254 ± 55	240 ± 70	378 ± 108	6710 ± 980 ^a
4 -IN-8		37 ± 4	9.4 ± 0.4	220 ± 25	n.a.
5S -IN-8		641 ± 126	n.a.	n.a.	n.a.
5R -IN-8		537 ± 131	n.a.	n.a.	n.a.
6S,S -IN-8		59 ± 4	n.a.	n.a.	n.a.
6R,R -IN-8		128 ± 3	n.a.	n.a.	n.a.

The p-c-Jun EC₅₀ values were determined with two different methods, by an HTRF based assay with a p-c-Jun(Ser63) antibody or by the classical western blot based method with a p-c-Jun-(Ser73) antibody; and the Pearson coefficient (0.68) calculated with the nine data points indicated a strong positive correlation between these two methods as expected. JNK activation was induced by doxycycline treatment in both cases and inhibitors were co-administered with the inducer and the respective p-c-Jun signal was measured after 6 h.

(Data show the mean ± parameter error estimate from weighted least squares method; for NanoBRET $n=2$; for other measurements $n=3$, independent experiments, except for ^a where $n=1$; n.a.: not available, not measured; x denotes that target engagement with NanoLuc-JNK1 could not be quantitatively measured due to lack of change in the BRET signal; Supplementary Fig. 1, 6, 7 and 8).

Table 2 | Crystallographic data collection and structural refinement

	JNK1-1aR-IN-8 ^b	JNK1-1aS-IN-8 ^b	JNK1-1a'R-IN-8 ^b
Data collection			
Space group	P3 ₁	P3 ₁	P3 ₁
Cell dimensions			
a, b, c (Å)	106.26, 106.26, 99.72	106.55, 106.55, 99.79	107.72, 107.72, 99.08
α, β, γ (°)	90, 90, 120	90, 90, 120	90, 90, 120
Resolution range (Å)	46.89-2.41	47.00-2.70	47.32-2.78
CC _{1/2}	0.999 (0.48)	0.999 (0.544)	0.999 (0.518)
R _{merge} ^a	0.073 (2.156)	0.102 (2.317)	0.094 (2.189)
I/σI	16.0 (0.9)	17.0 (1.2)	18.0 (1.4)
Completeness (%)	99.8 (98.2)	99.9 (100.0)	99.9 (99.9)
Redundancy	10.5 (7.3)	10.7 (10.8)	10.8 (10.8)
No. reflections	48522	34745	32333
Refinement			
R _{work} /R _{free}	0.2097 / 0.2262	0.2063 / 0.2256	0.2032 / 0.2179
No. atoms	8442	8391	8361
Protein	8277	8257	8215
Ligand/ion	138	132	141
Water	27	2	5
B-factors (Å ²)	84.37	89.09	93.04
Protein	84.50	89.10	92.93
Ligand/ion	79.43	88.34	99.53
Water	70.25	66.86	82.87
Ramachandran			
Favored (%)	97.03 %	96.92 %	96.00 %
Allowed (%)	2.88 %	3.08 %	4.00 %
Outliers (%)	0.10 %	0.00 %	0.00 %
R.m.s deviations			
Bond lengths (Å)	0.007	0.007	0.006
Bond angles (°)	1.048	1.035	1.005
PDB ID	8PTA	8PT9	8PT8

^aR_{merge} = $\sum_{hkl} \sum_i |I_i(hkl) - \langle I(hkl) \rangle| / \sum_{hkl} \sum_i I_i(hkl)$.

^bTwinning was present, -h,-k,l twinning operator was used during refinement.

Values in brackets are for the highest resolution bin.

The final crystallographic models contain three JNK1-small molecule complexes in the asymmetric unit.

described by k_3 and k_4 , respectively. To unambiguously determine all four parameters based on numerical fitting of the kinetic plots with the 2-step reversible kinetic model, k_1 and k_2 were first determined using the cysteine-to-serine mutated protein (JNK1 Cys116Ser). Reversible inhibitor potency ranking can be based on the steady-state inhibition constant, $K_i = (k_2/k_1) / (1 + (k_3/k_4))$ in molarity (M)³⁴. This analysis can also be used to estimate the energy contribution of reversible covalent bond formation for each inhibitor ($\Delta\Delta G$) (Supplementary Table 1).

The kinetic constants related to noncovalent binding (k_1 and k_2) varied only marginally as expected, since the common IN-8 moiety governs ATP-pocket binding for all inhibitors. In contrast, k_3 and k_4 , describing the contribution of the reversible covalent bond towards overall inhibitor behavior, greatly varied. In general, the reactivity of Michael acceptor – influenced by the presence of an electron-withdrawing ester group at C4, an ester vs amide at C2, ring strain (5- versus 6-membered ring) – correlated with inhibitor potency. The value of $\Delta\Delta G$, in addition to the above parameters, was also affected by the configuration at C4 (**1aR** vs **1aS**) and the relative positioning of the warhead compared to the directing IN-8 moiety (**1aR**-IN-8 vs **1a'R**-IN-8). Importantly, properly tuned and well-positioned cyclohexenone/

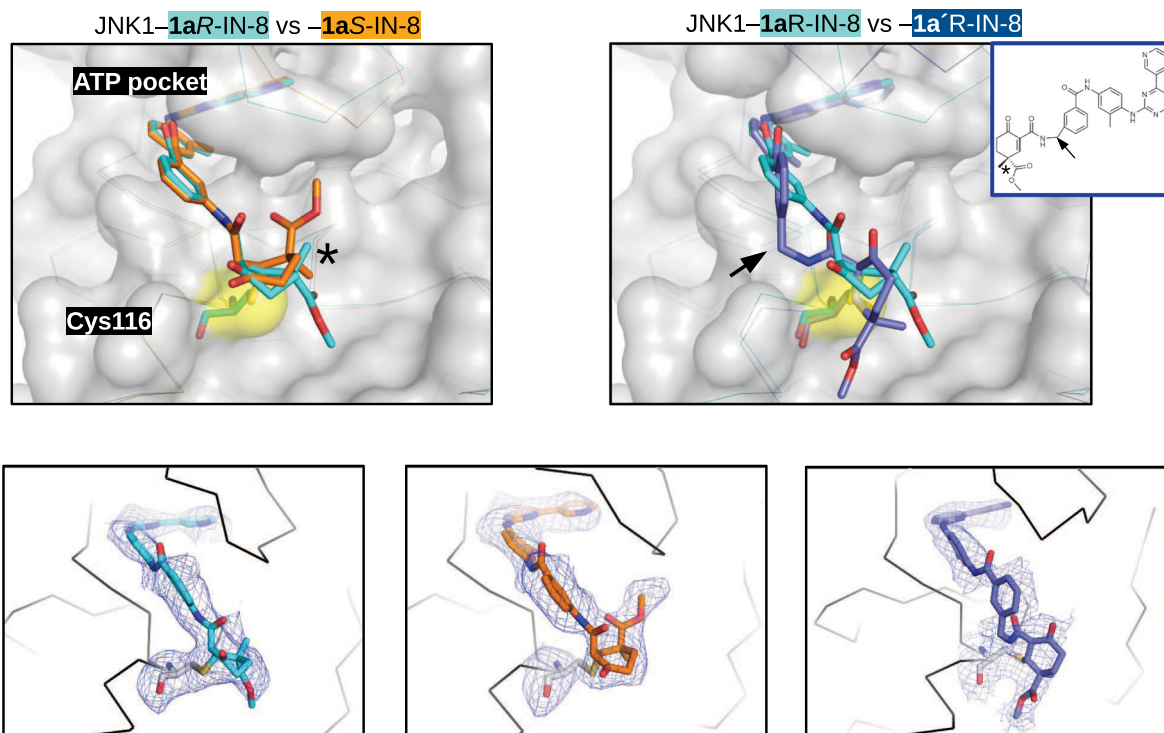
pentenone warheads all outperformed a similar and previously introduced cyanoacrylamide (CA) warhead design. The dissociation rate of the compounds (k_4) were lowered by about two orders of magnitude compared to k_2 , demonstrating that reversible covalent bond formation greatly increases occupancy as expected, provided that the warhead is positioned by the IN-8 directing moiety next to the cysteine thiol properly; otherwise k_4 drops close to k_2 (compare values for **1aR**-, **1a'R**-, and **1a'R**-IN-8) (see Supplementary Table 1). Inhibitor residence could also be tuned by further sterical crowding effects at C4 (**5S** vs **1aR**) or by the rigidity of the cyclohexenone ring (**6S,S** vs **1aR**). In agreement with this, further sterical crowding by the isopropyl group at C4 gave a JNK inhibitor that bound and dissociated fast (due to enhanced frustration upon thiol adduct formation), while the C4-C6 bridge slowed down both the association and the dissociation of the inhibitor (perfected for covalent residence) (see Supplementary Table 1). In summary, we showed that the binding affinity as well as the residence time of the composite JNK inhibitors could be adjusted and fine-tuned by varying the substitution pattern of the warhead scaffold and/or ring size.

JNK inhibitors in vitro and in cell-based tests

Further studies in vitro and in cell-based assays were conducted to compare reversible and irreversible JNK inhibitors (see Table 1). To test the inhibitory capacity of different inhibitors in vitro, a fast and quantitative assay for MAPK activity was developed which was based on the concept of phosphorylation assisted luciferase fragment complementation (PhALC)³⁵. JNK phosphorylates a protein construct containing a MAPK target motif (SENSOR) and phosphorylation of the target motif is recognized by the recognition construct (RC) containing a phosphoserine/threonine binding domain. The assay requires -1 μ M purified SENSOR and RC constructs and nanomolar concentration (1–5 nM) of phosphorylated JNK. The luminescence signal is generated by phosphorylation dependent luciferase complementation which is measured for 10–30 min giving a kinetic slope proportional to JNK activity. We used this assay to measure the inhibitory capacity (IC₅₀) of different covalent warhead containing JNK inhibitors in the presence of 10 mM GSH. In addition, some of the inhibitors' capacity to bind to the JNK1 ATP-pocket was also assessed by the NanoBRET target engagement assay in live HEK293T cells³⁶. Finally, interference with c-Jun phosphorylation was monitored by quantitative western blots in HEK293T cells (p-c-Jun IC₅₀). We also tested some additional covalent inhibitors using the PhALC assay. These contained varieties of the IN-8 ATP-binding moiety (IN-7, IN-9, and IN-10)²⁷ or a modified version of the IN-7 moiety in which one of the phenyl groups was replaced with a phenyl isostere, bicyclo[1.1.1]pentane, to improve physicochemical and pharmacological properties (**1aR**-isoPHEN)³⁷. These inhibitors performed similarly or slightly better compared to **1aR**-IN-8 in the PhALC assay (Table 3 and Supplementary Fig. 6).

The IC₅₀ value of irreversible JNK-IN-8 and reversible **1aR**-IN-8 on c-Jun phosphorylation triggered by 6 h of DOX stimulation in the engineered neuroblastoma cell line (SH-SY5Y MKK7 ACT; see Fig. 1d) was found to be similar (~0.7 μ M in the western blot based p-c-Jun(-Ser73) and ~100 nM in the HTRF p-c-Jun(Ser63) assay) (Supplementary Fig. 7 and 8). We noticed that specific JNK activation in this neuroblastoma cell line leads to decreased cell survival after 72 h, likely initiating cell death (Supplementary Fig. 9)^{23,38}. We then tested whether this JNK-specific response in this cell line could be blocked by the addition of JNK-inhibitors. It was found that reversible warhead-containing compounds (**1aR/S**, **1aR**-isoPHEN) as well as the irreversible JNK-IN-8 inhibitor protected cells from cell death to a significantly greater extent compared to IN-8 (i.e. the ATP competitive moiety alone). This showed that the reversible warhead could perform similarly to an irreversible one in this cellular setting and confirmed that covalent targeting indeed enhances the biological effect of a non-covalent directing group (IN-8) (Fig. 4a).

a



b

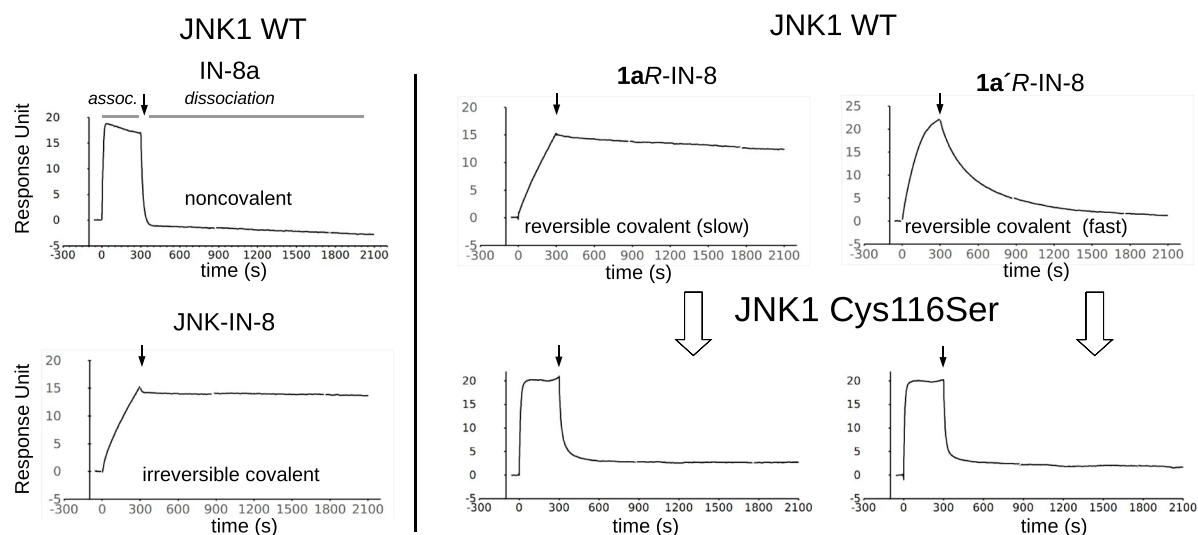


Fig. 2 | Crystal structures of covalent inhibitors bound to JNK1. **a** Structural comparisons of JNK1-**1aR**-IN-8, -**1aS**-IN-8, and -**1a'R**-IN-8 crystallographic complexes (with the following newly deposited PDB IDs: [8PTA](#), [8PT9](#), [8PTS](#), respectively). These show that the C4 stereogenic center could be used to direct the carboxymethyl group towards different directions in the substrate binding pocket next to Cys116 (left panel), or an additional methylene between the ATP-pocket binding moiety and the warhead necessitates a dramatically different conformational solution to form the cysteine covalent adduct (right panel). Lower panels display the Fo-Fc omit map for the cysteine-small molecule covalent adduct contoured at 1.5 σ . **b** Validation of the cysteine mediated covalent bond by SPR experiments. Mutation of Cys116 to serine increases the kinetic dissociation rate validating the importance of covalent bond formation upon binding. Panels show

the results of surface plasmon resonance (SPR) experiments with IN-8a (acetylated IN-8; noncovalent), JNK-IN-8 (irreversible covalent), **1aR**-IN-8 (reversible covalent, slow dissociation) and **1a'R**-IN-8 (reversible covalent, fast dissociation) binding to JNK1. Note that the association phase (assoc.) of the SPR curve is determined by the k_{on} , while the dissociation by the k_{off} . Compounds were injected over the JNK surface for 5 min at a concentration corresponding to their $-K_D$ and the dissociation of the JNK-compound complex or adduct was monitored in time (the start of the dissociation phase is shown with an arrow). Note that the kinetic binding profiles of **1aR**-IN-8 or **1a'R**-IN-8 on the JNK1 C116S surface resembles that of IN-8a (the ATP-pocket binding moiety without the warhead) on the wild-type (WT) JNK1 surface, suggesting that Cys116 is indispensable for the decreased k_{off} .

MAPKs are known to regulate gene expression by directly phosphorylating components of the AP-1 transcription factor (e.g., c-Jun, ATF or c-Fos)³⁹. The effect of JNK inhibitors on AP-1 mediated transcription was probed by using the AP-1 Reporter - HEK293 Recombinant Cell Line harboring an AP-1 promoter+luciferase reporter gene

cassette stably integrated into the genome. Promoter activity was stimulated by the addition of phorbol 12-myristate 13-acetate (PMA) and the transcription of the reporter gene was monitored by measuring luminescence after 6 h (where inhibitors were co-administered with PMA). According to these experiments, JNK-IN-8 showed similarly

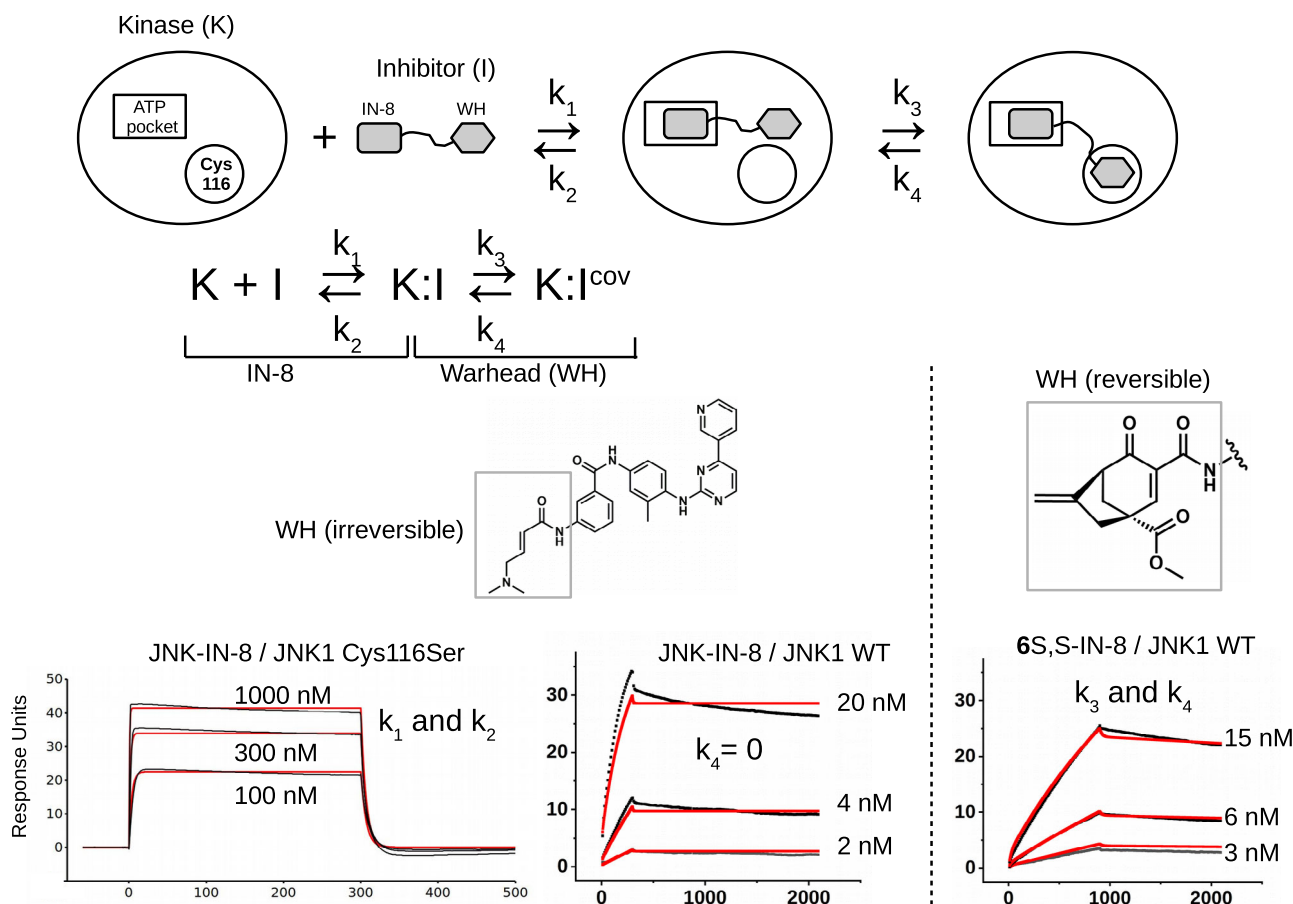


Fig. 3 | Inhibitor potency, binding energetics and covalent residence based on SPR data. Scheme of the 2-step reversible kinetic binding model showing the relevant kinetic binding constants for noncovalent binding via the IN-8 ATP-binding moiety (k_1 and k_2) and for warhead-mediated covalent bond formation (k_3 and k_4). The panels at the bottom show the kinetic binding plots for JNK-IN-8 on the JNK1(Cys116Ser) mutant surface injected at 100, 300, and 1000 nM concentrations (K_D - 200-300 nM) as well as the response curves on the wild-type JNK1 surface (WT) at three different concentrations. The analysis on the JNK1(Cys116Ser) mutant

surface gives the value of k_1 and k_2 based on a one-site noncovalent binding model; these values were independently determined for each inhibitor this way (see Supplementary Table 1). In the case of the irreversible JNK-IN-8 inhibitor $k_4 = 0$ (and thus only k_3 was fit), while for the reversible inhibitors k_3 and k_4 were both numerically fit to the experimental kinetic curves obtained on the JNK1 WT surface (and the panel on the right with 6S,S-IN-8 shows an example of this, for further data see Supplementary Fig. 5). The experimental binding curves are shown in black and the fitted curves in red.

weak inhibition as IN-8 (tested at 1, 3, and 10 μ M concentrations), while **1aR**-IN-8 and **1aR**-isoPHEN clearly caused stronger inhibition. Moreover, the reversible cyanoacrylamide warhead in CA-IN-8 could mediate only modest inhibition compared to the different cyclohexenone-based warheads from **5S**-, **6S,S**- and **1aR**-IN-8 (Fig. 4b).

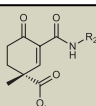
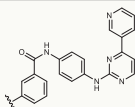
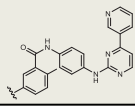
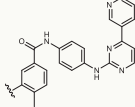
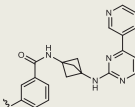
Earlier in vitro experiments showed that cyclohexenone/pentenone based warheads greatly decrease the k_{off} . To demonstrate that the reversible covalent warheads increase the cellular residence time as expected, we carried out cell-based wash-out experiments using the physiologically relevant AP-1 promoter-based reporter assay as well as the more direct NanoBRET target engagement assay. The inhibitors (IN-8a, JNK-IN-8, **1aR**-IN-8, **6S,S**-IN-8; 10 μ M) were washed out from AP-1 Reporter - HEK293 cells after 2 h of incubation and AP-1 promoter mediated luciferase reporter activity was measured after 6 h. These showed that all covalent inhibitors, in contrast to IN-8a, were indeed resilient to the wash-out as expected (Fig. 4c). Moreover, longer target engagement compared to IN-8a (noncovalent, N-acetylated IN-8 core) or even to CA-IN-8 (the reversible, cyanoacrylamide containing benchmark compound) was confirmed by similar wash-out experiments in HEK293T cells using the NanoBRET target engagement assay (Fig. 4d). In these latter experiments cells were first transiently transfected with a plasmid allowing the expression of the luciferase-JNK1 chimera construct. After 24 h cells were incubated with the different

inhibitors for two hours and washed three times before the fluorescent ATP-competitive tracer was added at different times after the wash-out (0, 4 and 8 h). The NanoBRET signal monitors the occupancy of the fluorescent dye on the target and reports on the level of free JNK1 (Supplementary Fig. 10). Results of these wash-out experiments suggest that reversible covalent bond formation greatly increases the in-cell residence time of cyclohexenone warhead containing inhibitors and, in contrast to the cyanoacrylamide containing inhibitor, the reversible warheads seem to be similarly as effective as the irreversible acrylamide warhead (at least up to the examined time, - 8 h).

Kinase specificity

MAPK specificity of reversible warhead containing inhibitors were assessed by using the PhALC assay, which showed that **1aR**-IN-8 has close to 1000-fold specificity towards JNK1 compared to p38 α or ERK2 (Supplementary Fig. 11a). Next, we tested the specificity of the inhibitors in cells. We used a cell line that allows p38-specific activation (HEK293T MKK6EE) and monitored MK2 substrate kinase phosphorylation with western blots using an anti-phosphoMK2 antibody⁴⁰. These experiments showed that **1aR**-IN-8, **1a'R**-IN-8, and **1a''R**-IN-8, similarly to JNK-IN-8, do not affect p38-mediated MK2 phosphorylation (Supplementary Fig. 11b). Finally, we tested if **1aR**-IN-8 may target a nearby surface cysteine (Cys163) located in the docking groove of JNK

Table 3 | Summary of in vitro JNK1 PhALC assay (with 10 mM GSH) results with compounds containing the same warhead with modified ATP-competitive fragments

	R ₂	PhALC IC ₅₀ /(nM)
1aR-IN-7		17 ± 5
1aR-IN-9		12 ± 1
1aR-IN-10		13 ± 2
1aR-isoPHEN		16 ± 2

(Data show the mean ± parameter error estimate from weighted least squares method; $n = 3$, independent experiments).

by using an in vitro fluorescence polarization-based protein-peptide binding assay. **1aR-IN-8** did not affect docking peptide binding, thus suggesting that the reversible inhibitors selectively interfere with JNK by specifically targeting its unique cysteine located next to the ATP binding pocket (Cys116 in JNK1) (Supplementary Fig. 11c).

Compared to an acrylamide based (acyclic) warhead moiety, the more complex (cyclic) structure around the α,β -unsaturated carbonyl in the cyclohexenone/pentenone scaffold could potentially lead to more selective cysteine targeting. Therefore, we tested the performance of **1aR-IN-8** on a large portion of the human kinome to assess its specificity towards JNKs. The compound was tested in 1 μ M concentration on the Wild Type Kinase Panel of Reaction Biology (comprised of 340 human kinases)^{36,41}. **1aR-IN-8** inhibited all three JNK isoforms (JNK1/2/3) as expected. In addition, this reversible compound also inhibited LIMK1 and TNK1 more than 50% (remaining activity: 38% and 44%, respectively), but all other kinases were mostly unaffected (Fig. 5a and Supplementary Table 2). This data suggests that **1aR-IN-8** is a uniquely specific JNK inhibitor. The modest inhibition of LIMK1 and TNK1 is presumably due to their surface cysteine located in their flexible P-loop that could be targeted by the warhead moiety and to good compatibility with the ATP-competitive moiety (IN-8) by their nucleotide binding pocket. In agreement to this, the corresponding close homologs (LIMK2 and ACK1/TNK2) that do not have a cysteine in their P-loop were less inhibited (remaining activity: 85% and 80%, respectively). Formerly, JNK-IN-8 was profiled in 1 μ M concentration using KINOMEScan methodology (DiscoverX, 442 distinct kinases)²⁷. This platform is quite different compared to the Reaction Biology platform, since the former employs an active site-directed competition binding assay to quantitatively measure interactions between test compounds and a kinase, while the latter quantitatively measures the compound's capacity to inhibit model substrate phosphorylation. There were 280 kinases common in the DiscoverX and Reaction Biology kinase panels and the inhibitory capacity of JNK-IN-8 and **1aR-IN-8** may be directly addressed on this common human kinase set. There were 23 kinases in the JNK-IN-8 dataset that were strongly bound by the irreversible acrylamide-based inhibitor (including the three JNKs and 20 off-target kinases). Importantly, **1aR-IN-8** with its reversible cyclohexenone-based warhead inhibited none of the 20 off-target

kinases (Supplementary Table 3). However, due to differences between the two kinome scan platforms, a direct comparison of these data sets may be misleading. To this end, we have chosen 6 kinases from the common set (the JNK3 target, and 5 off-target kinases: INSR, IRAK1, KIT, PDGFRB as off-targets from the JNK-IN-8 study and TNK1 as an off-target from the **1aR-IN-8** study) and an additional kinase, the homolog of TNK1 without a P-loop cysteine (ACK1/TNK2) and had them tested in the Eurofins DiscoverX platform at 1 μ M concentration with JNK-IN-8, **1aR-IN-8**, and **6S,S-IN-8**. All three inhibitors bound to the target JNK3 kinase well as expected (%Control was 0% for all three, where lower numbers indicate stronger interaction score). JNK-IN-8 had higher binding score for most off-targets, while **1aR-IN-8** performed better but off-target binding of **6S,S-IN-8** was even weaker (Fig. 5b). An explanation for the better performance of the latter two compounds against off-targets is provided below.

The Michael acceptor carbon atom is in a fundamentally different chemical environment in a cyclohexenone ring compared to an open-chain acrylamide-based warhead. Intuitively, the former has generally more limited accessibility and steric crowding groups will limit the spatial availability of the reactive carbon center for covalent adduct formation. This intuition is indeed supported by buried volume analysis where the accessibility of the reactive carbon was systematically analyzed in the most stable conformer⁴² (Fig. 5c, Supplementary Fig. 12, and Supplementary Note 1). Moreover, this comparative analysis on acrylamide (a1), cyanoacrylamide (b1) and cyclohexenone-(C2) amide (c1) – and their sterically crowded versions (e.g., *N,N*-dimethylacrylamide (a2), *tert*-butyl-cyanoacrylamide (b2), or (c2) 4,4-dimethyl-, (c3) 4-methyl-4-carboxymethyl-, (c4) 4-isopropyl-4-carboxymethyl-, and (c5) C4-C6-bridged-4-carboxymethyl-cyclohexenone-amide) – clearly suggested that the beta-carbon atom is notably hindered when the Michael acceptor moiety is in a substituted ring compared to acrylamide-based structures. In summary, in JNK TCIs the cyclic warheads could be used as somewhat different and more specific chemical solutions for nucleophile targeting compared to open-chain warheads.

JNK isoform specificity

Owing to the structure and inherent reactivity of the cyclic warheads, further structural modifications can be made to modulate selectivity of the composite compound. To generate additional compounds, the ester group at C4 was modified by using azide-alkyne cycloaddition and Sonogashira coupling. Accordingly, the methyl ester group was replaced with propargyl ester (**1bR-IN-8**, **1bS-IN-8**), which was further orthogonally extended by either CuAAC click chemistry (**1cR-IN-8**, **1cS-IN-8**) or by Sonogashira coupling (**1dR-IN-8**). Based on the crystal structure of the JNK1-**1aR-IN-8** complex, the pendant substituents at C4 were expected to project towards the shallow and wide substrate binding pocket of JNKs. Importantly, the propargyl ester was well-tolerated in this position, since **1bR-IN-8** showed a similar IC₅₀ value compared to that of **1aR-IN-8** in the PhALC assay or a similar EC₅₀ in the cell-based p-c-Jun phosphorylation assay (Fig. 6a,b). Intriguingly, JNK isoforms (JNK1/2/3), with some distinct functional roles in vivo and in cancer progression⁴³, show some sequence differences by the base of the substrate binding cleft. This latter is encoded by exon 6 which differs somewhat between the JNK isoforms (Fig. 6c and Supplementary Fig. 13). Notably, this -12 amino acid long region may also differ due to the alternative splicing of exon 6, which has an a and b form²³. In agreement to this, compounds derived from the propargyl ester derivatives and extended by azide-alkyne cycloaddition or Sonogashira coupling showed notable differences in JNK isoform specificity (measured for JNK2a2, JNK1b1 and JNK3a1, referred to below as JNK1, JNK2 and JNK3, respectively) (Supplementary Fig. 14). For example, inhibition of JNK1 was 10-fold higher compared to JNK2 by one of the two enantiomers of the propargyl ester derivative (**1bR-IN-8**), while **1cR-IN-8**, in which the more effective stereoisomer was further extended via azide-alkyne cycloaddition, had a more than tenfold selectivity

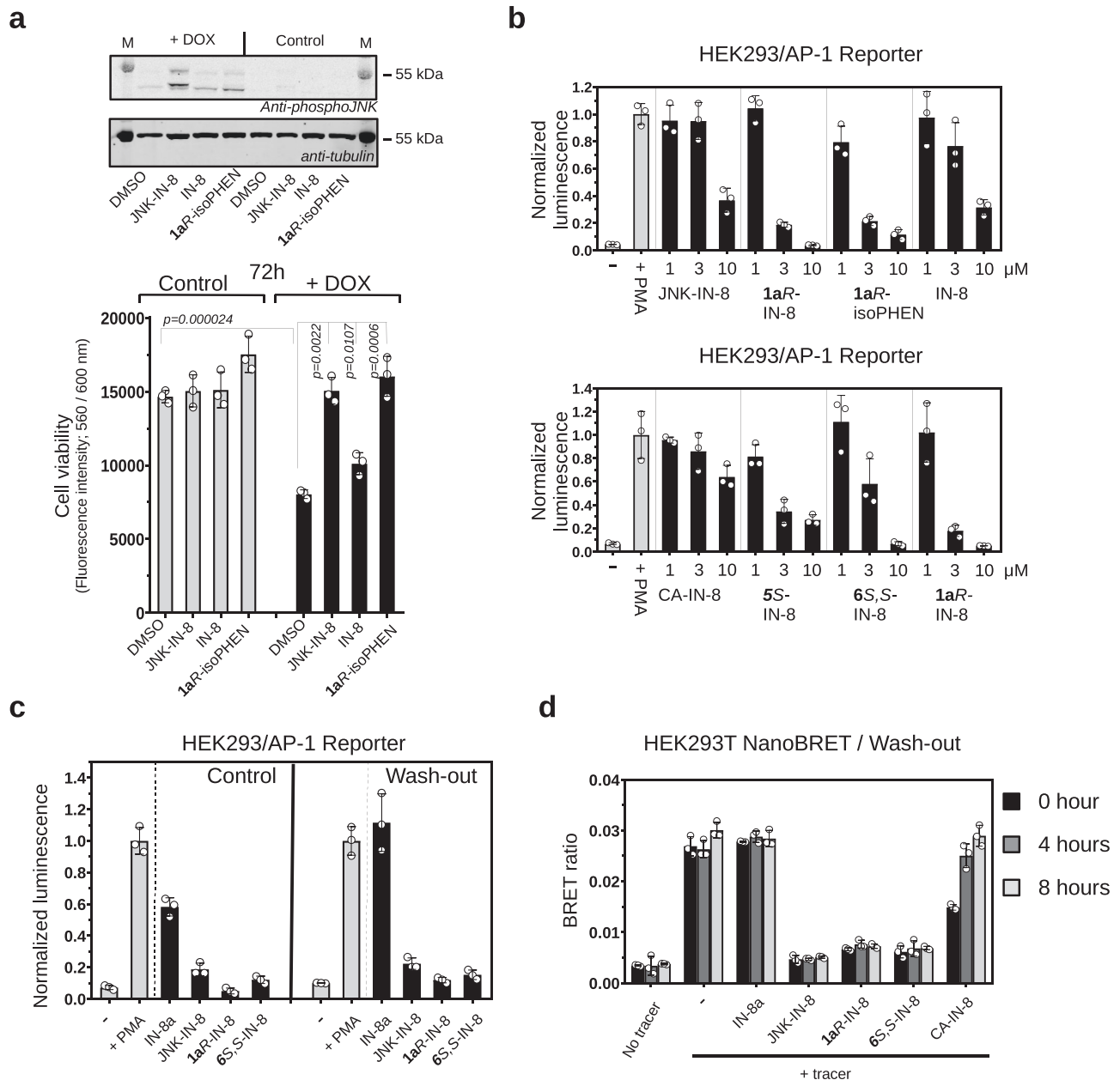


Fig. 4 | Characterization of covalent JNK inhibitors in cell-based tests. **a** Effect of inhibitors on JNK mediated cell death in SH-SY5Y MKK7 ACT cells. Endogenous JNK activation was initiated artificially by the addition of 2 μ g/mL doxycycline (DOX) for 72 h in engineered SH-SY5Y neuroblastoma cell line (in which the expression of an active MLK3-MKK7 chimera is controlled via the DOX dependent Tet-ON system). The top panel shows the results of a phospho-JNK western blot confirming JNK activation upon doxycycline treatment (+ DOX; the two different bands on the phospho-JNK western blot correspond to different JNK isoforms). The panel below shows the results of the experiment with 1 μ M JNK-IN-8 (irreversible), IN-8 (the ATP-pocket binding moiety without any warhead) or the reversible covalent 1aR-isoPHEN. (Data show the mean value and error bars show SD, $n=3$, independent experiments; p -values were calculated based on two-sided, unpaired t -test.) **b** Effect of inhibitors on JNK mediated AP-1 transcription factor promoter activity. Reporter AP-1 – HEK293 Recombinant Cell Line was unstimulated (-) or stimulated with phorbol 12-myristate 13-acetate (+ PMA) and AP-1 promoter driven transcription of the luciferase reporter gene was monitored by measuring luminescence after 6 h. Inhibitors were co-administered with PMA and were used in 1, 3, or 10 μ M concentrations. (Data show the mean and error bars show SD, $n=3$, independent experiments.) **c** Results of wash-out experiments with noncovalent (IN-8a), irreversible covalent (JNK-IN-8) and reversible covalent (1aR-IN-8 or 6S,S-IN-8)

inhibitors in the AP-1 promoter assay. Inhibitors (10 μ M) were incubated with Reporter AP-1 – HEK293 cells for 4 h then were left untreated (-) or stimulated with phorbol 12-myristate 13-acetate (+ PMA). AP-1 promoter activity was monitored by luminescence measurements after 6 h. Wash-out samples were washed by PBS twice before adding fresh media with PMA (but without any inhibitor), while for control cells the media, in addition to PMA, contained the respective inhibitor in the same concentration as before the wash-out. (Data show the mean and error bars show SD, $n=3$, independent experiments.) **d** Results of wash-out experiments monitoring long-term target engagement by NanoBRET. HEK293T cells were transiently transfected with a NanoLuc-JNK1 fusion expression plasmid and the binding of a fluorescent JNK ATP-pocket binding compound (tracer) was monitored in the absence or presence of different JNK inhibitors used in 10 μ M concentration. The BRET ratio is low when there was no tracer added (No tracer), while the maximum BRET signal is expected upon addition of the tracer with no inhibitor added (-). Cells were preincubated with the inhibitors for 2 h and washed three times with media followed by the addition of fresh media supplemented with the tracer. The remaining amount of the respective JNK-inhibitor complex was monitored by the BRET signal right after of the wash-out (0 h) or 4 and 8 h later. (Data show the mean and error bars show SD, $n=3$, independent experiments.) Source data are provided as a Source Data file.

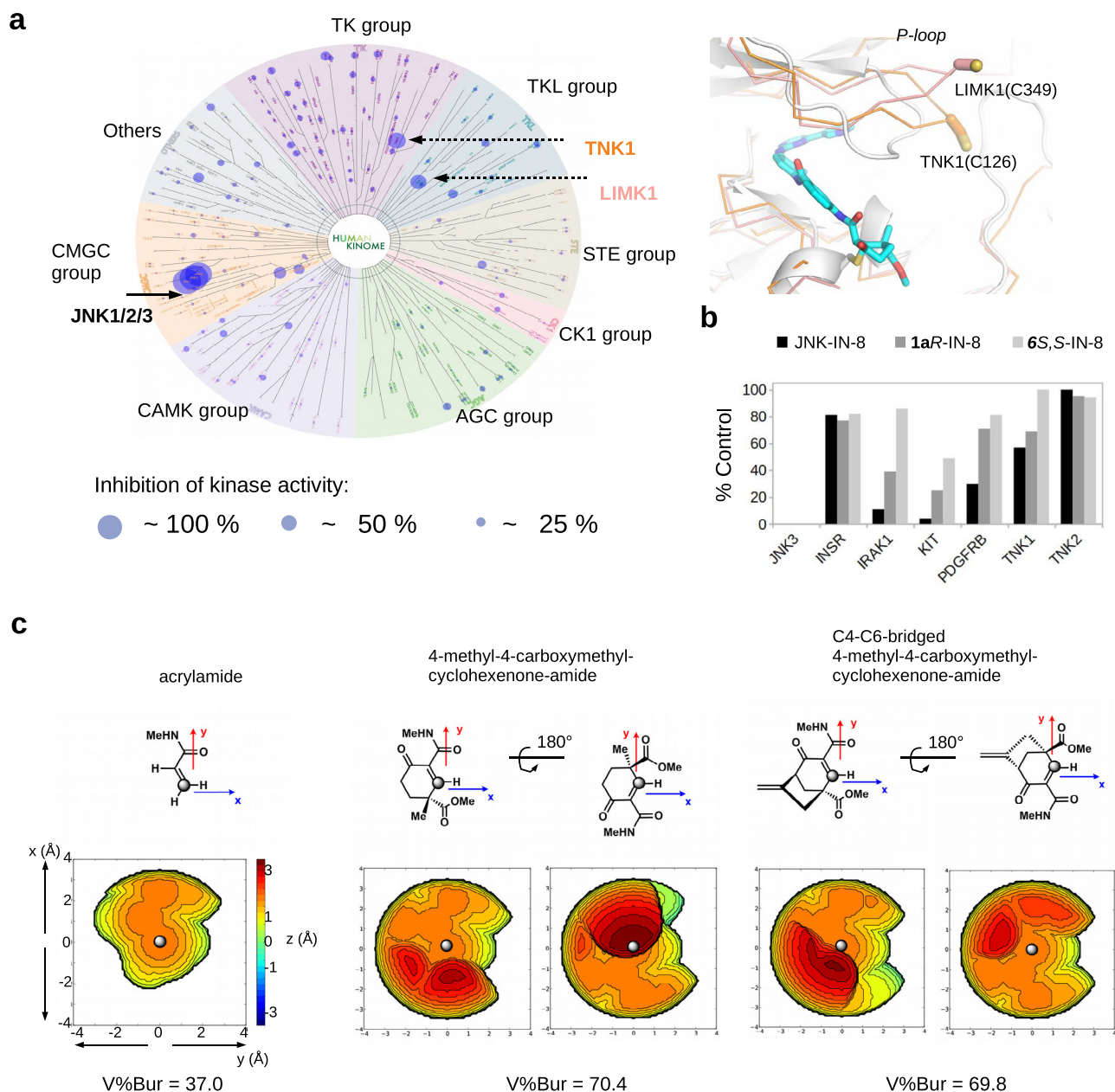


Fig. 5 | Specificity of 1aR-IN-8 in the human kinome panel and analysis of steric congestion near the reactive center of open-chain versus cyclic warheads.

a Results of the Wild Type Kinase Panel (Reaction Biology Corp. USA; 340 human kinases) with 1aR-IN-8 used at 1 μ M concentration. Inhibition of a specific kinase is depicted with a circle on the human kinome tree, where circle size correlates with the amount of inhibition. The panel on the right shows the structural models of LIMK1 (PDB ID: 3S95) and TNK1 (homology model created by AlphaFold 2) superimposed with the JNK1–1aR-IN-8 crystallographic model. LIMK1 and TNK1 are the only two human off-target kinases whose activity were inhibited more than 50% (see Supplementary Table 2). **b** Off-target kinase panel (1 target + 6 off-target kinases) and compound binding tested by the DiscoverX platform. Compounds were used in 1 μ M concentration. Note that JNK3 is the target kinase and interacted strongly with all three inhibitors (its %Control value is 0 for all three compounds which is invisible in the bar graph). For %Control lower numbers indicate stronger binding of the compound to the tested kinase (where 0 means complete binding

and 100 means no binding of the test compound to the kinase; the value shows the mean of duplicate measurements). (INSR: insulin receptor, IRAK1: interleukin 1 receptor associated kinase 1, KIT: c-KIT receptor tyrosine kinase, PDGFRB: platelet derived growth factor receptor beta, TNK1: tyrosine kinase non-receptor 1, TNK2: tyrosine kinase non-receptor 2, also known as ACK1). **c** Topographic steric maps of selected simplified warheads and buried volume calculation (V%Bur). Steric maps are derived from the DFT-optimized structures (see Supplementary Note 1). The isocontour scheme is in Å and a coloring scheme from dark red to deep blue is used to display sterically encumbered regions around the reactive center. The gray dot shown at the center of the xy plane represents the reactive carbon atom in the Michael acceptor and the steric map is viewed down the z-axis. Comparison of the steric maps of the simplified warheads indicates that the establishment of the cyclic form notably increases steric congestion and/or reshapes the encumbered region near the reactive center. Source data are provided as a Source Data file.

for JNK3 over JNK2. Overall, these findings lend support to the notion that reversible and bulkier cyclohexenone-based warheads may be well-suited to sense subtle structural differences around the targeted nucleophile, and thus they may also contribute to isoform specificity on their own right in TCIs.

Translational potential of JNK composite inhibitors

Synthetic elaboration of the cyclic warhead in composite JNK inhibitors is straightforward and varying substituent groups at C4 could be used to increase potency. For example, compared to a simpler design (1aR-IN-8), kinome-wide selectivity (see 1aR-IN-8 vs 6S,S-IN-8) or JNK isoform

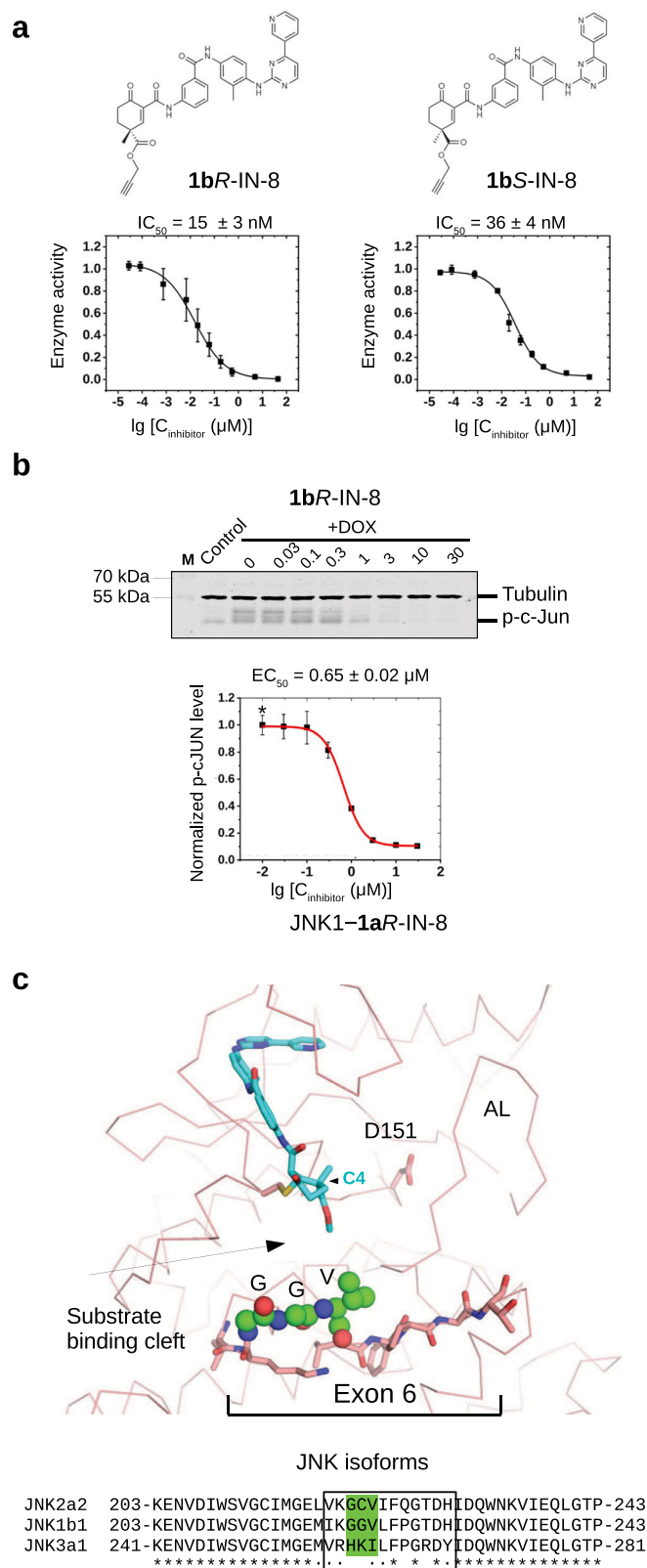


Fig. 6 | JNK isoform specificity of cyclohexenone warhead containing inhibitors. **a** PhALC assay results with **1bR**-IN-8 and **1bS**-IN-8. These compounds contain a propargyl ester moiety allowing further C4 extensions by either CuAAC click chemistry or by Sonogashira coupling (see Supplementary Fig. 14). Error bars show SD ($n = 3$, independent experiments). **b** Results of the in-cell c-Jun phosphorylation assay with **1bR**-IN-8. The Western-blot panel shows the results of one experiment. Data show the mean value and error bars show SD on the graph ($n = 3$, three independent experiments). Note that the EC_{50} of this modestly C4-extended compound displays similar inhibitory capacity compared to **1aR**-IN-8 (see Table 1). **c** The structural panel shows the crystal structure of the JNK1-**1aR**-IN-8 complex highlighting residues corresponding to exon 6 (shown with stick representation). This short region varies among JNK isoforms, and it forms the base of the substrate binding cleft next to the active site (D151). The three residues (GV) displaying the greatest variation among the examined JNK isoforms are shown with spheres on the structural panel. Note that the substrate binding cleft is remodeled upon JNK activation loop (AL) phosphorylation, but the region corresponding to exon 6, especially the residues shown with spheres, will stay in the proximity of the cyclohexenone warhead. Inhibitor contacts will likely be affected by the stereochemistry of the warhead and/or the length of the substituent groups at C4. Source data are provided as a Source Data file.

moieties in protein targeting chimeras (PROTACs) and to affect protein function by an independent mechanism, namely by lowering the cellular level of JNK. The **1aR**-IN-8 moiety was linked to a E3 ubiquitin ligase binding moiety specific for cereblon (CRBN) using a PEG-linker and a click chemistry-based (CuAAC) approach (**PRT_1**). This heterobifunctional molecule was effective in lowering the cellular level of JNK1 in HeLa cells in a proteasome-dependent manner (by ~65%), confirmed using the MG132 proteasome blocker compound, while p38 levels remained unaffected as expected (Supplementary Fig. 15). This shows that the C4 position of the cyclohexenone warhead is an easily variable exit point for different linkers and additional protein binding moieties even when these are introduced in the late stage of the synthesis.

According to our knowledge, the metabolic stability of double-activated cyclohexenone based compounds have not yet been tested. To this end, we examined the hepatic stability of **1aR**-IN-8 parallel to JNK-IN-8 using rat primary hepatocyte model. In addition, we also carried out the same analysis on a more simple warhead compound (**PK_test**), which was the C2 ester analogue of the warhead moiety present in **1aR**-IN-8 (referred to as compound **3** in ref. 29). Based on measured in vitro pharmacokinetics values (Cl_{int} in rat primary hepatocyte cultures), the in vivo hepatic clearance (Cl_H) in rat was predicted to be 10.1, 28.4 and 29.6 ml/min/kg for JNK-IN-8, **1aR**-IN-8, and **PK_test**, respectively (Supplementary Table 4)⁴⁴. According to this analysis, JNK-IN-8 was considered to have low, while **1aR**-IN-8 has intermediate hepatic extraction. Faster extraction of the latter is likely due to the warhead moiety, since **PK_test** was metabolized similarly to the composite **1aR**-IN-8 inhibitor. Next, we examined the stability of a more extended set of compounds using blood plasma from rats (see Supplementary Table 4). The half-life values of JNK-IN-8, **PK_test** and five composite JNK inhibitors, containing differently functionalized cyclohexenone warheads at C4, were determined from their depletion profiles by using mass spectrometry. Some of our warhead designs contained an ester at C4, which made the warhead more potent, but the known high esterase activity of blood plasma could decrease potency. The half-life values of ester containing compounds such as **PK_test**, **1aR**-IN-8, or **6S,S**-IN-8 were found to be indeed very short (a few minutes), while JNK-IN-8 or **2**-IN-8, containing no ester groups, were found to be stable in plasma. Importantly, the half-life could be greatly increased by extending the carboxymethyl group (**1cR**-IN-8) or replacing the C4 methyl group with a bulkier isopropyl group (**5S**-IN-8). Increased stability of these latter two compounds is likely due to their decreased compatibility with the reactive centers of blood esterases because of increased steric congestion at C4. In summary, this PK analysis demonstrated that the PK properties of the cyclic warheads could be greatly improved via simple synthetic elaboration of the core scaffold.

selectivity (see **1aR**-IN-8 vs **1bR**-IN-8), and even inhibitor efficacy on c-Jun substrate phosphorylation in cells (see Table 1), could be improved by changing the warhead scaffold at this accessible position. Moreover, the C4 of the rigid cyclohexenone ring appears to be an excellent exit vector for further synthetic elaboration of the warhead part of the inhibitors via click chemistry. This prompted us to test if these JNK binding compounds may also be used as JNK-specific

Discussion

We carried out a proof-of-concept study on the use of designer Michael acceptor covalent warhead with cyclic structure and extended 3D shape to inhibit JNKs, where an accessible cysteine located next to the ATP-pocket/substrate binding site was specifically targeted. These studies showed that the cyclohexenone/pentenone scaffold can be engineered to fine-tune binding affinity, residence time, and specificity by modifying steric and electronic properties of the warhead. For specific targeting, conjugation of the warheads to suitable non-covalent directing groups that fit into adjacent binding pockets is required in addition to introducing substituent groups at key ring positions. Such composite drugs with cyclic warheads can have greatly altered/enhanced properties compared to other cysteine targeting solutions. The warhead provides a synthetically feasible alternative to other irreversible or reversible covalent warheads (e.g., acrylamide or cyanoacrylamide) as it can be similarly linked to various directing groups: a *tert*-butyl group or IN-8 to direct it to the MAPK D-groove or next to the JNK ATP-pocket, respectively²⁹.

A comparative analysis showed that the cyclic warhead is comparable to, or may even supersede, its tested alternatives (irreversible acrylamide or reversible cyanoacrylamide) in the case of Cys116 in JNK1. Moreover, for the D-groove cysteine of ERK2 (Cys161), the cyclic warhead also performed better compared to its alternatives²⁹. The stereochemical requirements for covalent bond formation as well as for noncovalent contact compatibility are more rigorous and more specific around a Michael acceptor in a ring system compared to previously utilized acyclic warheads. Conversely, a more rigid, cyclic, and thus structurally more constrained reversible warhead may contribute more to binding affinity and specificity on its own right, far beyond that of a flexible, open-chain reversible covalent moiety (e.g. cyanoacrylamide). The advantage is more apparent when the cyclic warhead can target a cysteine in a surface pocket that matches up to its size and/or stereochemical configuration well. This positive selection mechanism is possibly the reason why cyclohexenone-based warheads were so efficient in targeting the MAPK D-groove cysteine²⁹. Conversely, the more complex ring structure can also hinder reactivity towards off-target cysteines due to higher probability for incompatibility with local surface topography (negative selection). In addition to less off-target effects, reversible cysteine engagement enables fine-tuning of inhibitor binding kinetics and thus residence time, which is a key feature in therapeutic applications requiring sustained target engagement⁴⁵, similarly to applications where more rapid target disengagement is more favorable⁴⁶.

According to the 2-step binding/reaction mechanism, the stable covalent complex forms via a more labile noncovalent complex (see Fig. 3), and for irreversible inhibitors k_4 (the kinetic dissociation constant of the covalent complex) is 0, while for reversible covalent inhibitors $k_4 > 0$. When the noncovalent complex first forms then this complex may dissociate fully (k_2) or progress to make the covalent complex (k_3). For reversible covalent JNK inhibitors, in vitro potency (K_i) is set mainly by the characteristics (k_3 , k_4) of the cyclohexenone/pentenone-based warhead designs (and the impact of k_1 or k_2 is relatively less since this is mainly governed by the ATP-pocket binding moiety shared by all inhibitors used for this comparison). In addition to the irreversible JNK-IN-8 reference compound, we also tested an open-chain reversible cyanoacrylamide based compound (CA-IN-8). In vitro characterization showed that this compound is also much more effective compared to its ATP-competitive directing moiety alone (IN-8 or IN-8a) as expected. However, this compound behaved poorly in most cell-based tests, particularly in the cell-based p-c-Jun phosphorylation assay. In summary, despite that CA-IN-8 could potentially form a strong, slowly dissociating covalent complex in a biochemical experiment (as in the dialysis experiments, see Fig. 1g), it is not as efficient as other composite JNK inhibitors with electronically similarly tuned cyclic Michael acceptors in the cell. Naturally, this could be due to inefficient

cellular uptake or to weakened binding to the signaling relevant pJNK-substrate complex because of its flexible aliphatic terminal appendage next to its reactive carbon but may also be due to higher reactivity of cyanoacrylamide compared to less reactive acrylamide. This higher reactivity may allow more (protein) off-target thiol interactions to take place causing a decrease in the effective cellular concentration compared to more rigid and specific cyclic Michael acceptors.

Another important finding of this comparative study is that a more rigid, cyclic reversible covalent warhead scaffold, if electronically properly tuned, may become similarly as effective as an irreversible covalent inhibitor. Additionally, we also demonstrated that the intrinsic reactivity (K_{chem}) of the reversible warhead scaffold in JNK composite inhibitors against free thiols is low and their reaction with GSH is dynamic and this off-target thiol adduct is only transient. Naturally, this is in stark contrast to an irreversible acrylamide-thiol adduct. Briefly, the transient nature of the reversible GSH adduct of the warhead scaffold is the mechanistic basis underlying their resilience to GSH in vitro as well as in cells.

We posit that the cysteine-targeting cyclic warhead complements and adds further specificity to the ATP-pocket binding moiety on its own right. Moreover, direct elaboration of properly oriented substituent groups through various orthogonal chemistries provides further opportunities for the design of more complex JNK inhibitors: these composite molecules distinguish even between some of the JNK isoforms, which remained elusive so far with conventional warheads. Moreover, reversible warhead containing JNK-specific compounds may also be used, in addition to their capacity to block JNK activity, to lower the cellular levels of JNKs as the key specificity component in JNK-specific PROTACs. This provides an additional modality to affect signaling protein function and the reversibility of the warhead could potentially be an advantageous property in such applications because JNK PROTACs can potentially be salvaged after proteosomal degradation of the adduct⁴⁸. The linker or the concrete structure of the ubiquitin ligase binding moiety are generally important for producing effective PROTACs, and the potency of a particular JNK PROTAC design may be optimized by varying these^{47,48}.

The pharmacokinetics of the compounds (e.g., hepatic and non-hepatic metabolism) need to be tested systematically, but our first characterization suggests that cyclohexenone-based warheads may have sufficient metabolic stability in vivo, moreover, their pharmacokinetic properties could be optimized in further work. Knowing that JNKs play the role of a double-edged sword in controlling many physiological processes, where too much or too less JNK activity or altered kinetics of the JNK response may all lead to pathological conditions depending on cell type, the capacity of being able to control the strength and/or the kinetics of cellular JNK inhibition via synthetic elaboration of the same reversible covalent scaffold will be a valuable asset in producing effective drugs against JNK-controlled diseases/processes (e.g. inflammation, neurodegeneration, cancer or resistance against chemotherapy).

In summary, the cyclic warhead scaffold provides a structural platform to fine-tune JNK inhibitor reactivity and selectivity by using different substitution patterns in rationally selected ring positions. We anticipate that our cyclic, structurally more complex warhead, which according to our knowledge previously had not been demonstrated as a practical solution to target cysteines on proteins, could be exploited far beyond the first two cases presented for the MAPK D-groove or for the JNK ATP-pocket²⁹.

Methods

Preparation of protein samples

Activated human ERK2, p38 α , JNK1 and JNK2 for the biochemical assays were produced by co-expressing the MAPKs with constitutively active GST-tagged MAP2Ks in *E. coli* with bicistronic plasmids (GST-MKK1_3D/ERK2, GST-MKK6_EE/p38 α , GST-MKK7_EE/JNK1/2)⁴⁹. Double

phosphorylation of the activation loop of MAPKs was confirmed in western blots with phosphoMAPK-specific antibody and/or mass spectrometry. MAPKs were expressed with an N-terminal His₆-tag that was cleaved off by the TEV protease after purification with Ni-NTA affinity resin, and then samples were further purified using ion-exchange chromatography (MonoQ, GE Healthcare). Dephosphorylated MAPKs were produced with GST-tagged λ-phage phosphatase and purified similarly. Human JNK3 was expressed alone using a simpler bacterial expression vector, and its activated form was produced by incubating the protein with constitutively active version of MKK7 in vitro before kinase activity measurements⁴⁹. GST-MKK7EE-His₆ was expressed in bacteria and double-affinity purified. Biotinylated JNK1 for the SPR experiments was co-expressed with the BirA ligase in *E. coli* and purified as described above but this construct retained an N-terminal AviTag after TEV cleavage. The JNK1 C116S mutant was generated by two-step PCR using DNA oligonucleotides to introduce the amino acid replacement (C116S_F: GCTCATGGATGCAA ATCTTAGCCAAGTGATTCAGATGGA and C116S_R: TCCATCTGAATC ACTTGGCTAAGATTTGCATCCATGAGC). Peptides were chemically synthesized using solid phase peptide synthesis (on Rink Amid resin, PS3 peptide synthesizer, Protein Technologies) with Fmoc^tBu strategy and purified by RP-HPLC using a Jupiter 300 Å C18 column (Phenomenex). Quality of the peptides were checked by HPLC-MS (Shimadzu LCMS-2020).

Dialysis experiments to confirm reversibility/irreversibility of different JNK-inhibitor complexes were done the following way. 50 nM phosphorylated JNK1 (p-JNK1) was incubated with 10 μM inhibitor in 50 mM HEPES pH = 7.4, 100 mM NaCl, 5 mM MgCl₂, 0.02% IGEPAL, 5 % glycerin, 5 mM TCEP, 0.5 mg/mL BSA (1 mL) for 1.5 h at room temperature, then samples were loaded into dialysis tubes and dialyzed in 50 mM HEPES pH = 7.4, 100 mM NaCl, 5 mM MgCl₂, 2 mM DTT. 50 μL aliquots were taken from the samples before the start of the dialysis experiment (0) and after the indicated times (1, 2, 3, 4, 5 days) and 5 μL were tested for enzymatic activity using the PhALC assay. The dialysis buffer (500 mL) was changed 2 h after the start of the experiment and then daily till the finish of the experiment. The control sample was treated the same way but no inhibitor was added in the incubation step before the dialysis experiment.

X-ray crystallography

For crystallographic analysis C-terminally truncated human JNK1_{ΔC20} was expressed in *E. coli* and purified with His₆-tag affinity, ion-exchange, and a gel-filtration step as described earlier⁴⁹. JNK1 was concentrated to 15 mg/ml, supplemented with 2 mM TCEP, and mixed in a 1:1.25 molar ratio with the inhibitors. Samples were crystallized in a hanging drop setup with 1 M NaCl in the reservoir. JNK1-1a'R-IN-8 crystals grew in 2–4 days in 8% PEG 3350, 0.1 M HEPES pH = 7.5 and the best crystals with JNK1-1aR-IN-8 or JNK1-1aS-IN-8 were grown in 12% PEG 3000, 2–4% MPD, 0.1 M HEPES pH=7.5. Crystals were flash-cooled in 25% glycerol. Data were collected at EMBL PETRA III beamline P14, Hamburg (see Table 2). Crystal structures were solved by molecular replacement using JNK as the search model from the JNK3-JNK-IN-7 crystallographic complex (PDB ID: 3V6S). The crystallographic models have three JNK1-inhibitor complexes in the asymmetric unit. Inhibitors were built using JLigand 1.0.40⁵⁰. Merohedral twinning was detected in the JNK1-inhibitor crystals (0.46, 0.45, 0.42 for JNK1-1aR-IN-8, -1aS-IN-8, and -1a'R-IN-8 calculated by PHENIX Xtriage, respectively) giving higher looking hexagonal symmetry, while the true space group proved to be P3₁. Structures were refined by using the -h, -k, l twin operator and NCS restraints with PHENIX⁵¹. The pose of the compounds regarding the functional groups at C4 was clear even from the beginning of the refinement for 1aR-IN-8, since the relative orientation of the methyl versus carboxymethyl groups could be decided based on unbiased maps even at the early stages of the refinement process. Due to somewhat poorer quality of the electron density map for 1aS-IN-8 or

for 1a'R-IN-8 the binding poses had to be decided by generating the different alternatives and analyzing the peaks in the Fo-Fc density maps. The two different stereoisomers emerging due to forming the C-S bond at C3 were drawn up in Jligand and whichever gave a better fit into the density was retained and the refinement was then finalized with the better fitting stereoisomer at C2 (since the covalent bond generates a new center at C2 as well). Density features were suitable to decide on the more likely stereoisomer at the A or B complexes. However, the asymmetric unit contains three different JNK-inhibitor adducts (A, B, C) and C was worse and had significantly higher B factors. Unfortunately, the density for this chain was not good enough to decide on the concrete stereochemistry at C2 and C3 without any bias. The stereoisomer from chain A and B were used to fit the weaker adduct density for C, therefore the final configurations in C need to be handled carefully for all JNK-inhibitor complexes.

Protein-peptide binding assay

Fluorescence polarization (FP) based protein-peptide binding experiments were used to assess binding into the MAPK docking groove⁴⁹. A known JNK docking groove binding peptide (evJIP1) was N-terminally labeled by carboxyfluorescein and 50 nM labeled reporter peptide was mixed with the MAPK in a concentration to achieve ~50–80% complex formation. The unlabeled competitor (peptide or small molecule) was added in increasing amounts and the FP signal was measured in a Cytation 3 (BioTek Instruments) fluorescence plate reader in 384-well plates in 20 μL volume. The K_d for the competitor was determined by fitting the data to a competition binding equation. Titration experiments were carried out in triplicates, and the average FP signal was used for fitting the data in Origin 2018⁴⁹.

In vitro kinase assay and in vitro IC₅₀ determination

The Phosphorylation-Assisted Luciferase Complementation assay (PhALC) was developed to measure JNK activity in vitro for fast and cost-effective identification/characterization of any compound blocking MAPK activity³⁵. The principle of this assay is the following: the general MAPK phosphorylation target motif (S/TP) is positioned C-terminal from a MAPK binding D-motif and this SENSOR construct is fused with the small fragment of the luciferase enzyme (NanoBiT small subunit, deep sea shrimp, *Oplophorus glacilirostris*, Promega). In the Recognition Construct (RC), the WW domain (from Pin1) binding specifically to the phosphorylated MAPK target motif is fused with the large fragment of the luciferase enzyme (NanoBiT large subunit)⁵². Upon SENSOR phosphorylation the RC will bind the SENSOR and triggers the assembly of the luciferase enzyme which will produce photons as it turns over its substrate (coelenterazine). Both constructs are produced with N-terminal maltose binding protein (MBP) and C-terminal histidine tag for high-yield bacterial expression and for simple affinity-resin purification. The two purified constructs (SENSOR and RC) were mixed with activated MAPKs, the reaction was started by injecting ATP into the reaction mix containing the luciferase enzyme substrate coelenterazine, and the luminescence signal was monitored in time. The PhALC assay was used as a semi-high throughput, microplate compatible biochemical assay to obtain IC₅₀ values of any compounds blocking MAPK activity. In more details: The PhALC constructs (SENSOR and RC) were expressed in *E. coli* using a modified pET expression vector (pET-MBP) and standard bacterial expression conditions in LB where the expression of proteins was induced by the addition of 0.2 mM IPTG at 25 °C for 4 h. Proteins were purified on Ni-NTA resin which was followed by another affinity purification step using maltose resin. RC and SENSOR were typically used in 1 μM concentrations with 1–10 nM double-phosphorylated MAPKs produced and purified as described earlier⁵³. The coelenterazine concentration was 200 μM and the reaction was started by adding 0.1 mM ATP. The kinase assay buffer contained 20 mM Tris pH = 8, 150 mM NaCl, 0.1% IGEPAL, 5 mM MgCl₂. The luminescence signal was monitored up to

30 min and the slope at the linear range (typically up to 5 min) was calculated based on linear regression. The p38 and ERK SENSOR contained the MEF2A D-motif (SRKPDLRVVIPP) and the JNK sensor had the more JNK-specific pepPDE4B motif (GDGISRPTTLPLTTLTLP)^{49,53}. SENSORS contained the same MAPK phosphorylation target sequence compatible with WW domain binding: VPRTPVS. This sequence motif was positioned C-terminal from the D-motif in SENSOR, separated by a flexible linker (HMGSSSGGSSGSGSVD). For IC₅₀ determination the competitor was added in increasing concentrations and the normalized slope of the luminescence signal was fitted to the dose-response equation in Origin 2018.

For the GSH resilience experiments the inhibitors were added in different concentrations into PhALC kinase assay buffer (without the ATP), the samples were incubated for 0, 6 or 18 h in the presence of 10 mM GSH before PhALC assay reagents were added (activated JNK1, SENSOR, and RC). The reaction was started by adding ATP. (The concentration of the inhibitors during incubation with 10 mM GSH was ~33% more compared to their final concentration used in the PhALC reaction mix). JNK enzymatic activity was measured as described above with the PhALC assay. (0 h incubation practically means -10 min, since this was the lag time of the measurement, i.e. before enzyme activity could be determined.)

Kinetic binding experiments

For surface plasmon resonance (SPR) measurements, biotinylated proteins were captured on a Biacore CAP sensor chip using a Biacore S200 instrument (GE-Healthcare). All measurements were done at room temperature using single-cycle setup with the standard Biacore method for CAP chip including double referencing. The K_D was determined based on response unit (RU) values corresponding to different concentrations of the analyte. Sensorgrams were fit to a 1:1 binding model using the BiaEvaluation software (GE Healthcare). The kinetic binding parameters (k_{off}) were determined from sensorgrams obtained at an analyte concentration corresponding to the equilibrium binding constant (K_D). The SPR running buffer was the following: 1 mM HEPES, 150 mM NaCl, 0.05 % TWEEN, 1 mM GSH, 1% DMSO. JNK1 was expressed biotinylated on an N-terminal AviTag in bacteria, purified, and immobilized on a Biacore CAP sensor chip. For more accurate kinetic analysis of covalent JNK inhibitors, the determination of k₁, k₂ (noncovalent k_{on} and k_{off}, respectively) and k₃, k₄ (covalent k_{on} and k_{off}, respectively) were done the following way. Inhibitors were injected over the JNK1(Cys116Ser) mutant surface at three different concentrations (100 nM, 300 nM, and 1000 nM) and this kinetic data was globally fit with to 1:1 binding model using the BiaEvaluation software (GE Healthcare), which gave the k₁ and k₂ value for each inhibitor. Next, the inhibitors were injected at three different concentrations (depending on their K_D determined earlier by independent equilibrium measurements) over the CAP sensor chip loaded with wild-type JNK1 and k₃ and k₄ values were determined by fitting the kinetic binding curves using the COPASI biochemical modeling software based on a 2-step reversible binding scheme, where k₁ and k₂ values were fixed⁵⁴.

To assess the precision of this quantitative analysis, we carried out the following parallel measurements and determined/calculated some of the parameters listed in Supplementary Table 1. 1) k₁ and k₂ were determined (100, 300, 1000 nM) for JNK-IN-8 on the JNK C116S surface (the values for this were 1492000 M⁻¹s⁻¹ and 0.1676 s⁻¹ compared to the results of the first measurement 1482000 M⁻¹s⁻¹ and 0.15360 s⁻¹, respectively, 2) k₃ for irreversible JNK-IN-8 was determined based on a second experiment (1, 3, 15 nM) on the JNK WT surface and it was calculated to be 0.03181 s⁻¹ (where the original value was 0.02952 s⁻¹) (moreover, using the newly determined k₁, k₂ a new k₃ based on the new experiment was calculated: 0.03454 s⁻¹), 3) k₃ and k₄ for the reversible covalent CA-IN-8 inhibitor were determined on the JNK WT surface based on two new experiments (a: 15, 40, 70 nM; b: 30, 60 nM) giving the following new values: a, k₃ = 0.01137 s⁻¹ and k₄ = 0.00033 s⁻¹;

b, k₃ = 0.01230 s⁻¹ and k₄ = 0.00035 s⁻¹ (and the original values were 0.01140 s⁻¹ and 0.00026 s⁻¹, respectively), 4) the k₃ and k₄ for **1aR**-IN-8 were calculated based on a new experiment (2, 5, 10 nM): k₃ = 0.02453 s⁻¹ and k₄ = 0.00035 s⁻¹ (and the values for the first experiment were 0.02617 s⁻¹ and 0.00034 s⁻¹, respectively), and finally 5) all four values for **6S,S**-IN-8 were determined based on new experiments (100, 300, 1000 nM on the JNK C116S and 3, 6 nM on the JNK WT surface): k₁ = 129000 M⁻¹s⁻¹, k₂ = 0.05387 s⁻¹, k₃ = 0.00630 s⁻¹, k₄ = 0.00004 s⁻¹ (and the original values were k₁ = 164000 M⁻¹s⁻¹, k₂ = 0.03460, k₃ = 0.01064, k₄ = 0.00006). We note that k₁ and k₂ values, which were determined based on the SPR experiments on the JNK C116S chip surface, are technically difficult to measure precisely since both kinetic parameters for the noncovalent mechanism are very fast (and thus give rapidly ascending or descending sensorgrams). Despite this, based on these measurements, the precision of the k₁₋₄ values listed in Supplementary Table 1 is good (~50 %) in the light of the technical challenges of the measurements and the complexity of the calculation.

Cell culture methods

50,000 HEK293T (ATCC, CRL-3216) cells were seeded into 24-well plates and were grown till confluence (typically 24 h) in 500 μl DMEM supplemented with 10 % FBS and were serum-starved (0% FBS) for 16 h before sorbitol (0.35 M) treatment for 15 min. The plate was put on ice and cells were resuspended, pelleted by centrifugation, and washed with ice cold PBS. The cell pellet was lysed in 80 μl 1X SDS-PAGE loading buffer, 10 μl was loaded onto 10% Tris-glycine SDS-PAGE gels and gels were blotted to nitrocellulose membrane. Inhibitors (1 μl dissolved in 50 % DMSO) were added 2 h before sorbitol treatment. SH-SY5Y MKK7 ACT cells (created from SH-SY5Y, ATCC CRL-2266; see later), allowing specific activation of JNK upon addition of an inducer, were handled similarly but JNK activation was induced by the addition of 3 μg/ml doxycycline. Inhibitors (1 μl dissolved in 50% DMSO) were added together with doxycycline and samples were harvested for western blot analysis as described above. Western blot results were analyzed using Odyssey CLx imaging system (Li-Cor) and fluorescently labeled secondary antibodies: IRDye 680RD (Goat anti-mouse IgG; Li-cor #926-68070; 1:0000) or IRDye 800CW (Goat anti-rabbit IgG, Li-Cor #926-32211; 1:5000). The primary antibodies were the following: anti-phospho JNK (Cell Signaling #9251; 1:1000), anti-phospho-c-Jun(Ser73) (Cell Signaling #9164; 1:1000), anti-phospho p38 (Cell Signaling #9215, 1:3000), anti-phospho MK2 (Cell Signaling #3007, 1:1000), anti-α-tubulin (Sigma #T6199; 1:10000), or anti-FLAG (Sigma #F1804; 1:10000). Anti-α-tubulin antibody was used as the load control and the anti-FLAG antibody was used to monitor the expression of the transgene responsible for specific MAPK activation.

The HEK293T MKK6EE cell line (allowing p38-specific activation by doxycycline inducible expression of the constitutively active upstream activator kinase, MK6EE) was described earlier⁴⁰. The SH-SY5Y (neuroblastoma; ATCC CRL-2266) MKK7 ACT cell line was generated using lentiviral transduction with an MKK7(ACT)-MLK3 construct containing full-length human MKK7 fused to the kinase domain of human MLK3 (aa. 117-379). The generated Tet-ON inducible stable cell line was evaluated by time dependent transgene induction and downstream target phosphorylation upon doxycycline treatment in DMEM F12 (Gibco) media supplemented with 1% FBS, as described earlier^{31,40}. For the determination of JNK inhibitor mediated c-Jun phosphorylation, cells were stimulated with 2 or 3 μg/mL doxycycline (DOX), co-administered with different amounts of inhibitors, and samples were subjected to quantitative western blot (WB) analysis after 6 h. To obtain the EC₅₀ value, the normalized phospho-c-Jun WB signal was fitted with the DoseResponse function of Origin 2018. For the p-c-Jun HTRF measurements -40,000 SH-SY5Y MKK7 ACT cells were seeded into a 96-well plate in DMEM F12 + 1% FBS and the HTRF Phospho-c-Jun(Ser63) Detection Kit (#64JUNPEG, PerkinElmer) was

used to measure the level of phosphorylated c-Jun after 6 h of DOX treatment. To obtain the IC₅₀ value, the HTRF ratio (emission at 665 / emission at 620 nm) was fitted with the DoseResponse function of Origin 2018. The HTRF signal was measured using a BioTek Cytation 3 multi-mode reader equipped with an HTRF measuring cube (Europium cypate donor / Red acceptor readout setup; Agilent Technologies).

The PrestoBlue Cell Viability Reagent (ThermoFisher, P50200) was used to assess cell viability. 3,000 SH-SY5Y MKK7 ACT cells were plated in 96-well plates in DMEM with 10% FBS. Next day the medium was changed for new media (DMEM with 0.1% of FBS) and cells were incubated with inhibitors for 72 h. The medium was then removed and PrestoBlue reagent was added to live cells, incubated for 45 min, and then the fluorescence signal (ex: 560 nm, em: 600 nm) was measured in a plate reader. Linearity of the detection was checked in a parallel experiment where control cells were serially diluted, and the signal was measured according to the manufacturer's protocol.

20,000 Reporter AP-1 – HEK293 cells (BPS Bioscience, #60405) were seeded into a 96-well plate in 100 µl DMEM (Gibco) supplemented with 10% FBS. After cells become adherent (confluency: 80%) the inhibitors were added in Opti-MEM (Gibco) supplemented with 1% FBS and following 2 h of incubation cells were stimulated with 6 ng/ml PMA solution for 6 h. The luminescence signal was read out using a BioTek Cytation 3 microplate reader after adding freshly prepared Steadylite Plus solution (PerkinElmer) according to the manufacturer's protocol. For the wash-out experiments cells were similarly handled but washed three times with Opti-MEM + 1% FBS (100 µl) before adding 100 µl fresh media with 6 ng/ml PMA solution without any inhibitor for 6 h (Wash-out). Control cells were treated the same way but the fresh media after the wash-out contained the original inhibitors and PMA.

For the experiments with the photocaged **1aR-IN-8** compound, Reporter AP-1 – HEK293 cells were seeded into a microplate as described above. Cells were pre-treated with the inhibitor in the dark (DARK plate) two hours before stimulation with anisomycin. The LIGHT plate was treated differently: 30 min after inhibitor addition, the plate was subjected to four cycles of illumination (15 s) and recovery (30 s) with blue light ($\lambda = 450$ nm) using a custom-made led illumination device allowing water cooling of the plate (output power: 210 mW)⁵⁵, and then cells were incubated in the dark for 1.5 h. Cells from the DARK and LIGHT plates were then stimulated with 10 µg/mL anisomycin for 30 min to turn JNK activity on, lysed with SDS loading buffer, and prepared for western blot analysis. Uncaging of Photocaged **1aR-IN-8** by illumination was confirmed in vitro (see Supplementary Fig. 2).

NanoBRET assay

The NanoBRET target engagement assay was carried out by Reaction Biology Corp (Malvern, USA; 4000 cells/well, 384-well format) or performed by us (40,000 cells/well, 96-well format) according to the protocol of the NanoBRET® TE Intracellular Kinase Assays (#N2500, Promega) using the NanoLuc-MAPK8 fusion vector with the K5 tracer (see Supplementary Fig. 1). Briefly, HEK293 cells were transfected with JNK1 and transfection carrier DNA (1:9). The transfected cells were treated with compounds (8–10-dose with 3-fold dilution starting at 1, 10 or 100 µM). JNK1 target engagement was measured by NanoBRET assay. The K-5 tracer concentration was 0.5 µM. Compound treatment time was 2 h. To obtain the EC₅₀ value, the normalized BRET response (normalized BRET ratio to untreated cells) was fitted with the DoseResponse function of Origin 2018.

In the wash-out experiments the NanoLuc-MAPK8 fusion vector (NV1701, Promega) was transfected into HEK293T cells using Lipofectamine 3000 (Invitrogen), otherwise the nanoBRET measurement was carried out according to the protocol of the supplier (NanoBRET Target Engagement Intracellular Kinase Assay, adherent format) using the K-10 tracer (0.4 µM). 40,000 transfected cells were seeded into a 96-well plate and after 24 h cells were preincubated with inhibitors for

2 h, washed 3 times with 100 µl Opti-MEM + 1% FBS before adding fresh media to cells (see Supplementary Fig. 10). The BRET ratio (emission 650 nm/emission 450 nm) was measured using a BioTek Cytation 3 multi-mode reader equipped with a nanoBRET cube (#8040592, Agilent Technologies).

Kinase specificity profiling

The human kinase specificity profile of **1aR-IN-8** was tested by Reaction Biology Europe GmbH (Freiburg, Germany) using the Wild Type Kinase Panel comprised of 340 active human kinases. Briefly, profiling was done using the ³³PanQinase™ assay which measures the inhibition of phosphorylation of kinase substrate peptides in a radioactive assay format⁴⁰. The data is given as per cent remaining activity compared to the control experiment without the inhibitor. The inhibitor was used in 1 µM concentration and ATP was used at a concentration matching its apparent K_M for each kinase. Test compound, kinase, ATP, and a natural substrate peptide for each kinase were incubated in FlashPlate microtiter plates (PerkinElmer) coated with a scintillant. Reactions were stopped after one hour. Assays were carried out in duplicates. The off-target kinase panel was tested by Eurofins DiscoverX® Products LLC (Fremont, US) using the ScanELECT service on the indicated kinases at 1 µM compound concentration. The assay was carried out in duplicates according to the KINOMEScan procedure as described earlier⁵⁶.

Mass spectrometry

The molecular weights of the conjugates of GSH were identified using a Triple TOF 5600+ hybrid Quadrupole-TOF LC/MS/MS system (Sciex, USA) equipped with a DuoSpray IonSource coupled with a Shimadzu Prominence LC20 UFLC (Shimadzu, Japan) system consisting of quaternary pump, an autosampler and a thermostated column compartment. Data acquisition and processing were performed using Analyst TF software version 1.7.1 (Sciex). Chromatographic separation was achieved on a Phenomenex Luna Omega PS C18 (50 mm × 2,1 mm, 3 µm, 100 Å) HPLC column. Sample was eluted in gradient elution mode using solvent A (0.1% formic acid in water) and solvent B (0.1% formic acid in ACN). The initial condition was 10% B followed by a linear gradient to 55% B by 12 min, to 95% B by 3 min, 15 to 17.5 min 95% B was retained; and from 17.5 to 18 min back to initial condition with 10% eluent B and retained from 18 to 20 min. Flow rate was set to 0.4 ml/min. The column temperature was 40 °C and the injection volume was 5 µl. UV-VIS spectrometer was used at 254 nm wavelength. Nitrogen was used as the nebulizer gas (GS1), heater gas (GS2), and curtain gas with the optimum values set at 30, 30 and 35 (arbitrary units), respectively. Data were acquired in positive electrospray mode in the mass range of m/z = 300 to 2500, with 1 s accumulation time. The source temperature was 350 °C and the spray voltage was set to 5500 V. Declustering potential value was set to 80 V. Peak View Software™ V.2.2 (Sciex) was used for deconvoluting the raw electrospray data to obtain the neutral molecular masses.

The procedure described above allowed the identification of the irreversible GSH–JNK-IN-8 adduct only. For the identification of the reversible GSH–**1aR-IN-8** adducts the LC step had to be shortened and the details of these differences are described below. For this adduct there was only a short separation carried out and samples were only retained on a short security guard cartridge (Phenomenex C18, 4 × 3 mm, Phenomenex, USA). The goal of this solution was focusing and desalting the protein samples prior to ionization. A 4 min gradient (both in solvent composition and flow rate) was used with initial flow of 0.5 mL/min and 10% eluent B. This was held for 0.5 min for washing out the salts from the sample. A 1.5 min linear increase was applied to reach the final flow of 1 mL/min and maximum eluent composition of B at 65%. These parameters were held for 0.5 min and a quick 0.1 min linear gradient was used to reach the initial flow rate and eluent composition. This was followed by a 1.4 min equilibrating part. Water containing 0.1% formic acid (eluent A) and acetonitrile containing 0.1% formic

acid) were used for chromatography. The injected volumes were 5 μ L. The wavelength in UV detection was 280 nm. The MS step was carried out similarly as described above.

NMR measurements on covalent adduct formation

NMR experiments were conducted on a Varian NMR System spectrometers operating at 600 MHz. Off-target adduct formation was analyzed through the reaction between **1aR**-IN-8 and beta-mercaptoethanol (BME) by ^1H NMR. All reagents were dissolved and the experiments were carried out in PBS (D_2O , pH ~7.2) with 75% DMSO. Details of the measurements, the assignment of the spectra and K_{chem} determination are described in Supplementary Note 2.

Pharmacokinetic analysis

In vitro pharmacokinetic behaviour of the JNK inhibitors was determined in rat (Wistar) plasma and primary hepatocytes. Blood plasma and hepatocytes isolated from male Wistar rats were obtained from Toxi-Coop Toxicological Research Centre Ltd. (Budapest, Hungary). Primary hepatocytes were isolated by using collagenase perfusion method of Bayliss and Skett⁵⁷. Briefly, the liver tissues were perfused through the portal vein with Ca^{2+} -free medium (Earle's balanced salt solution) containing EGTA (0.5 mM) and then with the same medium without EGTA, finally with the perfusate containing collagenase (Type IV, 0.25 mg/ml) and Ca^{2+} at physiological concentration (2 mM). The yield and percent of cell viability according to the trypan blue exclusion test were determined⁵⁸.

Time courses of the unchanged JNK inhibitors (JNK-IN-8, **1aR**-IN-8 and PK_{test}) in primary hepatocytes were obtained. Each compound was incubated with cell suspension (2×10^6 cells/ml) at 37 °C in a humid atmosphere containing 5 % CO_2 . The parent compounds dissolved in dimethylsulphoxide (DMSO) were added directly to the cell culture medium (William's E medium: Ham's F12 medium=1:1) at the final concentration of 1 or 10 μ M. The final concentration of DMSO was 0.1%. At various time points (at 0, 10, 20, 30, 60, 90, 120, 180, 240 min), the incubation mixtures were sampled (aliquots: 0.1 ml) and terminated by the addition of ice-cold acetonitrile (0.3 ml). JNK inhibitors were also incubated in cell-free medium and sampled at 0 and 240 min. The samples were centrifuged and analyzed by LC-MS/MS for quantitation of the parent compound (Supplementary Note 3). Intrinsic clearance (Cl_{int}), the in vitro pharmacokinetic parameter was calculated from the decrease in the concentration of the parent compound, whereas the in vivo parameters (hepatic clearance Cl_{H} , hepatic extraction ratio E , bioavailability F) were predicted from Cl_{int} according to the previously published method⁵⁸. The cut-off value of hepatic extraction ratio between low and intermediate was considered to be 0.3, whereas 0.7 between intermediate and high extraction compounds.

Time courses of the JNK inhibitors (JNK-IN-8, **1aR**-IN-8, **2**-IN-8, **5S**-IN-8, **1cR**-IN-8, **6S**,**S**-IN-8 and PK_{test}) in rat plasma were also obtained. The parent compounds dissolved in DMSO were added directly to the blood plasma at the final concentration of 1 or 10 μ M. At various time points (at 0, 10, 20, 30, 60, 120 min), the incubation mixtures were sampled (aliquots: 0.05 ml) and terminated by the addition of 0.15 ml ice-cold acetonitrile. The samples were centrifuged and analyzed by LC-MS/MS for quantitation of the parent compound, and elimination half-life values ($t_{1/2}$) were calculated from the decrease in the concentration of the parent compound.

Characterization and synthesis of small molecules

All reactions were carried out using oven-dried glassware and anhydrous solvents unless noted otherwise. Flash silica chromatography was performed on silica gel (ZEOPrep 60 25-40 μ m, ZEOCHEM) with the indicated eluents. Reverse phase chromatography was performed using a gradient method on a Gemini[®] 5 μ m C18 110 Å column (H_2O :MeCN = 95:5 (0.1% HCOOH) to 100% MeCN (0.1% HCOOH)). Thin-layer chromatography was performed on silica plates (Kieselgel 60

F254 Merck). Compounds on TLC were visualized by UV (254 nm) or KMnO_4 or p-anisaldehyde staining. Chemical shifts are referenced to the residual solvent signals (CHCl_3 : δ = 7.26 ppm for ^1H , δ = 77.0 ppm for ^{13}C ; DMSO: δ = 2.50 ppm for ^1H , δ = 39.5 ppm for ^{13}C ; CH_3OH : δ = 4.87 ppm and 3.31 ppm for ^1H , δ = 49.0 ppm for ^{13}C). Data are reported as follows: chemical shifts (ppm), multiplicity (s = singlet, d = doublet, t = triplet, q = quartet, sept. = septet, br = broad, m = multiplet, dd = doublet of doublets, ddd = doublet of doublet of doublets, dddd = doublet of doublet of doublet of doublets, dt = doublet of triplets, ddt = doublet of doublet of triplets, td = triplet of doublets), coupling constants (Hz), and integration. All spectra were recorded with the standard spectrometer pulse sequences and settings using a Varian 300, 500 and 600 MHz spectrometer. The enantiomeric excess of the products was determined on a chiral stationary phase HPLC (Daicel Chiralpak ID 250 \times 4.6 mm, 5 μ m column) using Hexane:iPrOH=9:1 as eluent. All starting materials were purchased from Aldrich, TCI, or Fluorochem and used without further purification unless stated otherwise. Anhydrous THF and toluene were distilled from sodium/benzophenone, while anhydrous DMF and DMSO were kept under Ar on 4 Å molecular sieves.

JNK-IN-8 was purchased from Selleck Chemicals. The synthetic procedures for compounds and intermediates thereof used in this study (e.g., IN-8, IN-8a, CA-IN-8, **1aR**-IN-8, **1aS**-IN-8, Photocaged **1aR**-IN-8, **1a'R**-IN-8, **1a''R**-IN-8, **2**-IN-8, **3**-IN-8, **4**-IN-8, **5S**-IN-8, **5R**-IN-8, **6S**,**S**-IN-8, **6R**,**R**-IN-8, **1a**'-IN-7, **1aR**-IN-9, **1aR**-IN-10, **1aR**-isoPHEN, **1bR**-IN-8, **1bS**-IN-8, **1cR**-IN-8, **1cS**-IN-8, **1dR**-IN-8) are described in Supplementary Note 4.

Reporting summary

Further information on research design is available in the Nature Portfolio Reporting Summary linked to this article.

Data availability

Crystal structures of JNK1-**1aR**-IN-8, -**1aS**-IN-8, and -**1a'R**-IN-8 are deposited in the Protein Data Bank with accession codes **SPTA**, **SPT9**, and **SPT8**. The following X-ray structures are available from the PDB: **3V6S**, **2ERK** and **3S95**. Source data are provided with this paper.

References

- Boike, L., Henning, N. J. & Nomura, D. K. Advances in covalent drug discovery. *Nat. Rev. Drug Discov.* **21**, 881–898 (2022).
- Roskoski, R. Orally effective FDA-approved protein kinase targeted covalent inhibitors (TCIs). *Pharmacol. Res.* **165**, 105422 (2021).
- Krishnan, S. et al. Design of reversible, cysteine-targeted michael acceptors guided by kinetic and computational analysis. *J. Am. Chem. Soc.* **136**, 12624–12630 (2014).
- Gehring, M. & Laufer, S. A. Emerging and Re-Emerging Warheads for Targeted Covalent Inhibitors: Applications in Medicinal Chemistry and Chemical Biology. *J. Med. Chem.* **62**, 5673–5724 (2019).
- Resnick, E. et al. Rapid Covalent-Probe Discovery by Electrophile-Fragment Screening. *J. Am. Chem. Soc.* **141**, 8951–8968 (2019).
- Liu, Q. et al. Developing irreversible inhibitors of the protein kinase cysteinome. *Chem. Biol.* **20**, 146–159 (2013).
- Miller, R. M. & Taunton, J. Targeting protein kinases with selective and semipromiscuous covalent inhibitors. *Methods Enzymol.* **548**, 93–116 (2014).
- Zhao, Z., Liu, Q., Bliven, S., Xie, L. & Bourne, P. E. Determining Cysteines Available for Covalent Inhibition Across the Human Kinome. *J. Med. Chem.* **60**, 2879–2889 (2017).
- Chaikwad, A., Koch, P., Laufer, S. A. & Knapp, S. The Cysteinome of Protein Kinases as a Target in Drug Development. *Angew. Chem. - Int. Ed.* **57**, 4372–4385 (2018).
- Jackson, P. A., Widen, J. C., Harki, D. A. & Brummond, K. M. Covalent Modifiers: A Chemical Perspective on the Reactivity of

- α,β -Unsaturated Carbonyls with Thiols via Hetero-Michael Addition Reactions. *J. Med. Chem.* **60**, 839–885 (2017).
- Klaeger, S. et al. The target landscape of clinical kinase drugs. *Science* **358**, eaan4368 (2017).
 - Lanning, B. R. et al. A road map to evaluate the proteome-wide selectivity of covalent kinase inhibitors. *Nat. Chem. Biol.* **10**, 760–767 (2014).
 - Serafimova, I. M. et al. Reversible targeting of noncatalytic cysteines with chemically tuned electrophiles. *Nat. Chem. Biol.* **8**, 471–476 (2012).
 - Bradshaw, J. M. et al. Prolonged and tunable residence time using reversible covalent kinase inhibitors. *Nat. Chem. Biol.* **11**, 525–531 (2015).
 - Spradlin, J. N., Zhang, E. & Nomura, D. K. Reimagining Druggability Using Chemoproteomic Platforms. *Acc. Chem. Res.* **54**, 1801–1813 (2021).
 - Ullah, R., Yin, Q., Snell, A. H. & Wan, L. RAF-MEK-ERK pathway in cancer evolution and treatment. *Semin. Cancer Biol.* **85**, 123–154 (2022).
 - Fu, L., Chen, S., He, G., Chen, Y. & Liu, B. Targeting Extracellular Signal-Regulated Protein Kinase 1/2 (ERK1/2) in Cancer: An Update on Pharmacological Small-Molecule Inhibitors. *J. Med. Chem.* **65**, 13561–13573 (2022).
 - Lavoie, H., Gagnon, J. & Therrien, M. ERK signalling: a master regulator of cell behaviour, life and fate. *Nat. Rev. Mol. Cell Biol.* **21**, 607–632 (2020).
 - Davis, R. J. Signal Transduction by the JNK Group of MAP Kinases. *Cell* **103**, 239–252 (2000).
 - Johnson, G. L. & Nakamura, K. The c-Jun Kinase/Stress-activated Pathway: Regulation, Function and Role in Human Disease. *Biochim. Biophys. Acta* **1773**, 1341 (2007).
 - Canovas, B. & Nebreda, A. R. Diversity and versatility of p38 kinase signalling in health and disease. *Nat. Rev. Mol. Cell Biol.* **22**, 346–366 (2021).
 - Wagner, E. F. & Nebreda, Á. R. Signal integration by JNK and p38 MAPK pathways in cancer development. *Nat. Rev. Cancer* **9**, 537–549 (2009).
 - Zeke, A., Misheva, M., Reményi, A. & Bogoyevitch, M. A. JNK signaling: Regulation and functions based on complex protein-protein partnerships. *Microbiol. Mol. Biol. Rev.* **80**, 793–835 (2016).
 - Schellino, R., Boido, M. & Vercelli, A. JNK Signaling Pathway Involvement in Spinal Cord Neuron Development and Death. *Cells* **8**, 1576 (2019).
 - Duong, M. T. H., Lee, J. H. & Ahn, H. C. C-Jun N-terminal kinase inhibitors: Structural insight into kinase-inhibitor complexes. *Comput. Struct. Biotechnol. J.* **18**, 1440–1457 (2020).
 - Bogoyevitch, M. A. & Arthur, P. G. Inhibitors of c-Jun N-terminal kinases: JuNK no more? *Biochim. Biophys. Acta* **1784**, 76–93 (2008).
 - Zhang, T. et al. Discovery of potent and selective covalent inhibitors of JNK. *Chem. Biol.* **19**, 140–154 (2012).
 - Meister, A. Glutathione metabolism and its selective modification. *J. Biol. Chem.* **263**, 17205–17208 (1988).
 - Póti, A. L. et al. Targeting a key protein-protein interaction surface on mitogen-activated protein kinases by a precision-guided warhead scaffold. *Nat. Commun.* <https://doi.org/10.1038/s41467-024-52574-1> (2024).
 - Bogoyevitch, M. A., Ketterman, A. J. & Sugden, P. H. Cellular stresses differentially activate c-Jun N-terminal protein kinases and extracellular signal-regulated protein kinases in cultured ventricular myocytes. *J. Biol. Chem.* **270**, 29710–29717 (1995).
 - Kirsch, K. et al. Co-regulation of the transcription controlling ATF2 phosphoswitch by JNK and p38. *Nat. Commun.* **11**, 5769 (2020).
 - Tang, X. J. et al. Photorelease of Pyridines Using a Metal-Free Photoremovable Protecting Group. *Angew. Chem. Int. Ed. Engl.* **59**, 18386–18389 (2020).
 - Deslongchamps, P. Reactions on SP² type unsaturated systems. in *Stereoelectronic Effects in Organic Chemistry* 221–241 (Pergamon Press Ltd, 1983).
 - Mons, E., Roet, S., Kim, R. Q. & Mulder, M. P. C. A Comprehensive Guide for Assessing Covalent Inhibition in Enzymatic Assays Illustrated with Kinetic Simulations. *Curr. Protoc.* **2**, e419 (2022).
 - Póti, Á. L. et al. Phosphorylation-Assisted Luciferase Complementation Assay Designed to Monitor Kinase Activity and Kinase-Domain-Mediated Protein-Protein Binding. *Int. J. Mol. Sci.* **24**, 14854 (2023).
 - Anastassiadis, T., Deacon, S. W., Devarajan, K., Ma, H. & Peterson, J. R. Comprehensive assay of kinase catalytic activity reveals features of kinase inhibitor selectivity. *Nat. Biotechnol.* **29**, 1039–1045 (2011).
 - Stepan, A. F. et al. Application of the bicyclo[1.1.1]pentane motif as a nonclassical phenyl ring bioisostere in the design of a potent and orally active γ -secretase inhibitor. *J. Med. Chem.* **55**, 3414–3424 (2012).
 - Le-Niculescu, H. et al. Withdrawal of survival factors results in activation of the JNK pathway in neuronal cells leading to Fas ligand induction and cell death. *Mol. Cell. Biol.* **19**, 751–763 (1999).
 - Whitmarsh, A. J. & Davis, R. J. Transcription factor AP-1 regulation by mitogen-activated protein kinase signal transduction pathways. *J. Mol. Med. (Berl.)* **74**, 589–607 (1996).
 - Sok, P. et al. MAP Kinase-Mediated Activation of RSK1 and MK2 Substrate Kinases. *Structure* **28**, 1101–1113.e5 (2020).
 - Wang, Y. & Ma, H. Protein kinase profiling assays: a technology review. *Drug Discov. Today Technol.* **18**, 1–8 (2015).
 - Falivene, L. et al. Towards the online computer-aided design of catalytic pockets. *Nat. Chem.* **11**, 872–879 (2019).
 - Bogoyevitch, M. A. The isoform-specific functions of the c-Jun N-terminal Kinases (JNKs): differences revealed by gene targeting. *Bioessays* **28**, 923–934 (2006).
 - Tóth, K. et al. Utility of in vitro clearance in primary hepatocyte model for prediction of in vivo hepatic clearance of psychopharmacons. *Microchem. J.* **136**, 193–199 (2018).
 - Copeland, R. A. The dynamics of drug-target interactions: drug-target residence time and its impact on efficacy and safety. *Expert Opin. Drug Discov.* **5**, 305–310 (2010).
 - Knockenbauer, K. E. & Copeland, R. A. The importance of binding kinetics and drug-target residence time in pharmacology. *Br. J. Pharmacol.* <https://doi.org/10.1111/BPH.16104> (2023)
 - Gabizon, R. et al. Efficient Targeted Degradation via Reversible and Irreversible Covalent PROTACs. *J. Am. Chem. Soc.* **142**, 11734–11742 (2020).
 - Bemis, T. A., La Clair, J. J. & Burkart, M. D. Unraveling the Role of Linker Design in Proteolysis Targeting Chimeras. *J. Med. Chem.* **64**, 8042–8052 (2021).
 - Garai, A. et al. Specificity of linear motifs that bind to a common mitogen-activated protein kinase docking groove. *Sci. Signal.* **5**, ra74 (2012).
 - Lebedev, A. A. et al. JLigand: a graphical tool for the CCP4 template-restraint library. *Acta Crystallogr. D. Biol. Crystallogr.* **68**, 431–440 (2012).
 - Adams, P. D. et al. The Phenix software for automated determination of macromolecular structures. *Methods* **55**, 94–106 (2011).
 - Dixon, A. S. et al. NanoLuc Complementation Reporter Optimized for Accurate Measurement of Protein Interactions in Cells. *ACS Chem. Biol.* **11**, 400–408 (2016).
 - Zeke, A. et al. Systematic discovery of linear binding motifs targeting an ancient protein interaction surface on MAP kinases. *Mol. Syst. Biol.* **11**, 837 (2015).
 - Hoops, S. et al. COPASI - A COMplex PATHway Simulator. *Bioinformatics* **22**, 3067–3074 (2006).

55. Egyed, A. et al. Turning Red without Feeling Embarrassed-Xanthonium-Based Photocages for Red-Light-Activated Phototherapeutics. *J. Am. Chem. Soc.* **145**, 4026–4034 (2023).
56. Fabian, M. A. et al. A small molecule-kinase interaction map for clinical kinase inhibitors. *Nat. Biotechnol.* **23**, 329–336 (2005).
57. Bayliss, K. M. & Skett, P. Isolation and culture of human hepatocytes. in *Human Cell Culture Protocols* (ed. Jones, G. E.) 369–390 (Humana Press, 1996).
58. Berry, M. N. et al. Initial determination of cell quality. in *Isolated Hepatocytes* 45–47 (Elsevier, 1991).

Acknowledgements

This work was supported by the National Research Development and Innovation Office (NKFIH) grants (KKP 126963 awarded to A.R., NKFIH-PD-135121 awarded to M.B., NKFIH-PD-146252 awarded to D.C., and NKFIH-K-142486 awarded to I.P.), VEKOP-2.3.3-15-2016-00011, and by the Hungarian Academy of Sciences (KEP-10/2019), and by the National Research, Development and Innovation Fund (2020-1.1.2-PIACI-KFI-2020-00021 awarded to K.M.). We acknowledge support at the EMBL beamlines at PETRA III storage ring, Hamburg. The authors are thankful to Krisztina Németh for HRMS measurements. A.R. is thankful to Marie Bogoyevitch for useful discussions on JNKs in the early phases of the project.

Author contributions

Á.L.P., D.B., T.S. and A.R. conceived of the project idea, made intellectual contributions, designed experiments, analyzed and interpreted the data and wrote the manuscript. D.B., L.T. and R.P. synthesized compounds, Á.L.P. characterized the compounds by biochemical measurements, A.A. and E.SZ. carried out cell-based assays and K.A. did SPR measurements. P.S. determined the crystal structures and I.B. collected X-ray data. D.C. and I.P. carried out the theoretical buried volume calculations. M.B. synthesized the photocaged **1aR**-IN-8 compound and D.F.-N. characterized it in cells. F.F. and K.M. carried out in vitro pharmacokinetic studies in rat hepatocytes and plasma. G.T. carried out the NMR measurements required for the analysis of the off-target BME adduct. T.I. and P.SZ. carried out MS measurements.

Competing interests

A.R., T.S., Á.L.P., D.B., A.A., P.S., L.T., K.A., T.I., E.SZ. and R.P. are inventors in a patent application pending approval (PCT/HU2023/050079) on the

use of cyclic designer scaffolds for the covalent targeting of proteins via Michael addition. The remaining authors declare no competing interests.

Additional information

Supplementary information The online version contains supplementary material available at <https://doi.org/10.1038/s41467-024-52573-2>.

Correspondence and requests for materials should be addressed to Tibor Soós or Attila Reményi.

Peer review information *Nature Communications* thanks the anonymous reviewers for their contribution to the peer review of this work. A peer review file is available.

Reprints and permissions information is available at <http://www.nature.com/reprints>

Publisher's note Springer Nature remains neutral with regard to jurisdictional claims in published maps and institutional affiliations.

Open Access This article is licensed under a Creative Commons Attribution-NonCommercial-NoDerivatives 4.0 International License, which permits any non-commercial use, sharing, distribution and reproduction in any medium or format, as long as you give appropriate credit to the original author(s) and the source, provide a link to the Creative Commons licence, and indicate if you modified the licensed material. You do not have permission under this licence to share adapted material derived from this article or parts of it. The images or other third party material in this article are included in the article's Creative Commons licence, unless indicated otherwise in a credit line to the material. If material is not included in the article's Creative Commons licence and your intended use is not permitted by statutory regulation or exceeds the permitted use, you will need to obtain permission directly from the copyright holder. To view a copy of this licence, visit <http://creativecommons.org/licenses/by-nc-nd/4.0/>.

© The Author(s) 2024